

1 |  
2 An updated synthesis of ocean total alkalinity and dissolved inorganic carbon measurements  
3 from 1993 to 2023: the SNAPO-CO2-v2 dataset  
4

5 Nicolas Metzl<sup>1</sup>, Jonathan Fin<sup>1,2,3</sup>, Claire Lo Monaco<sup>1</sup>, Claude Mignon<sup>1</sup>, Samir Alliouane<sup>4</sup>, Bruno Bombled<sup>5</sup>,  
6 Jacqueline Boutin<sup>1</sup>, Yann Bozec<sup>6</sup>, Steeve Comeau<sup>4</sup>, Pascal Conan<sup>7,8</sup>, Laurent Coppola<sup>4,8</sup>, Pascale Cuet<sup>9</sup>, Eva  
7 Ferreira<sup>5</sup>, Jean-Pierre Gattuso<sup>4,10</sup>, Frédéric Gazeau<sup>4</sup>, Catherine Goyet<sup>11</sup>, Emilie Grossteffan<sup>12</sup>, Bruno Lansard<sup>5</sup>,  
8 Dominique Lefèvre<sup>13</sup>, Nathalie Lefèvre<sup>1</sup>, Coraline Leseurre<sup>14</sup>, Sébastien Petton<sup>15</sup>, Mireille Pujon-Pay<sup>8</sup>, Christophe  
9 Rabouille<sup>5</sup>, Gilles Reverdin<sup>1</sup>, Céline Ridame<sup>1</sup>, Peggy Rimmelin-Maury<sup>12</sup>, Jean-François Ternon<sup>16</sup>, Franck  
10 Touratier<sup>11</sup>, Aline Tribollet<sup>1</sup>, Thibaut Wagener<sup>13</sup>, Cathy Wimart-Rousseau<sup>17</sup>.

11  
12 <sup>1</sup> Laboratoire LOCEAN/IPSL, Sorbonne Université-CNRS-IRD-MNHN, Paris, 75005, France

13 <sup>2</sup> OSU Ecce Terra, Sorbonne Université-CNRS, Paris, 75005, France

14 <sup>3</sup> Now at Institut des Sciences de la Terre, Grenoble, 38058, France

15 <sup>4</sup> Sorbonne Université, CNRS, Laboratoire d'Océanographie de Villefranche, LOV, F-06230 Villefranche-sur-  
16 Mer, France

17 <sup>5</sup> Laboratoire des Sciences du Climat et de l'Environnement, LSCE/IPSL, UMR 8212 CEA- CNRS-UVSQ,  
18 Université Paris-Saclay, 91191 Gif-sur-Yvette, France

19 <sup>6</sup> Station Biologique de Roscoff, UMR 7144 – EDYCO-CHIMAR, Roscoff, France

20 <sup>7</sup> Sorbonne Université, CNRS, Laboratoire d'Océanographie Microbienne, LOMIC, F-66650 Banyuls-sur-Mer,  
21 France

22 <sup>8</sup> Sorbonne Université, CNRS OSU STAMAR - UAR2017, 4 Place Jussieu, 75252, Paris cedex 05, France

23 <sup>9</sup> Laboratoire ENTROPIE and Laboratoire d'Excellence CORAIL, Université de La Réunion-IRD- CNRS-  
24 IFREMER-Université de la Nouvelle-Calédonie, 97744, Saint-Denis, La Réunion, France

25 <sup>10</sup> Institute for Sustainable Development and International Relations, Sciences Po, 27 rue Saint Guillaume, F-  
26 75007 Paris, France

27 <sup>11</sup> Espace-Dev UMR 228 Université de Perpignan Via Domitia, IRD, UM, UA, UG, 66860, Perpignan, France

28 <sup>12</sup> Institut Universitaire Européen de la Mer (OSU-IUEM), Univ Brest, CNRS-UAR3113, 29280, Plouzané,  
29 France

30 <sup>13</sup> Aix Marseille Univ, Université de Toulon, CNRS, IRD, MIO, Marseille, France

31 <sup>14</sup> Flanders Marine Institute (VLIZ), 8400 Ostend, Belgium

32 <sup>15</sup> Ifremer, Univ Brest, CNRS, IRD, LEMAR, F-29840 Argenton, France

33 <sup>16</sup> MARBEC, Univ Montpellier, CNRS, Ifremer, IRD, Sète, France

34 <sup>17</sup> National Oceanography Centre Southampton, European Way, Southampton, SO14 3ZH, UK  
35

36 *Correspondence to:* Nicolas Metzl (nicolas.metzl@locean.ipsl.fr)  
37

38 **Abstract.** Total alkalinity ( $A_T$ ) and dissolved inorganic carbon ( $C_T$ ) in the oceans are important properties to  
39 understand the ocean carbon cycle and its link with global change (ocean carbon sinks and sources, ocean  
40 acidification) and ultimately find carbon based solutions or mitigation procedures (marine carbon removal). We  
41 present an extended database (SNAPO-CO2, Metzl et al, 2024d) with 24700 new additional data for the period  
42 2002 to 2023. The full database now includes more than 67000  $A_T$  and  $C_T$  observations along with basic  
43 ancillary data (time and space location, depth, temperature and salinity) in various oceanic regions obtained since  
44 1993 mainly in the frame of French research projects. This includes both surface and water columns data  
45 acquired in open oceans, coastal zones, rivers and in the Mediterranean Sea and either from time-series or  
46 punctual cruises. Most  $A_T$  and  $C_T$  data in this synthesis were measured from discrete samples using the same  
47 closed-cell potentiometric titration calibrated with Certified Reference Material, with an overall accuracy of  $\pm 4$   
48  $\mu\text{mol kg}^{-1}$  for both  $A_T$  and  $C_T$ . The same technique was used onboard for underway measurements during cruises

49 conducted in the Southern Indian and Southern Oceans. The  $A_T$  and  $C_T$  data from these cruises are also added in  
50 this synthesis. The data are provided in one dataset for the global ocean (<https://doi.org/10.17882/102337>) that  
51 offers a direct use for regional or global purposes, e.g.  $A_T$ /Salinity relationships, long-term  $C_T$  estimates,  
52 constraint and validation of diagnostics  $C_T$  and  $A_T$  reconstructed fields or ocean carbon and coupled  
53 climate/carbon models simulations, as well as data derived from Biogeochemical-Argo (BGC-Argo) floats.  
54 These data can also be used to calculate pH, fugacity of  $CO_2$  ( $fCO_2$ ) and other carbon system properties to derive  
55 ocean acidification rates or air-sea  $CO_2$  fluxes.

56

## 57 **1 Introduction**

58

59 The ocean plays a major role in reducing the impact of climate change by absorbing more than 90% of  
60 the excess heat in the climate system (Cheng et al., 2020, 2024; von Schuckmann et al, 2023; IPCC, 2022) and  
61 about 25% of human released  $CO_2$  (Friedlingstein et al., 2022, 2023). In the last decade, the oceans experienced  
62 a rapid warming, the year 2023 being the hottest since 1955 (Cheng et al, 2024). In the atmosphere the  $CO_2$   
63 concentration continues its terrific progressive rising, reaching 419.3 ppm in 2023 (a rate of  $+2.83 \text{ ppm yr}^{-1}$ , Lan  
64 et al 2024). In August 2024, the global atmospheric  $CO_2$  concentration was already above 420 ppm. In the next  
65 decade the oceans will continue to capture heat and  $CO_2$ , somehow limiting the climate change, but this oceanic  
66  $CO_2$  uptake changes the chemistry of seawater reducing its buffering capacity (Revelle and Suess, 1957; Jiang et  
67 al, 2023). This process known as ocean acidification has potential impacts on marine organisms (Fabry et al.,  
68 2008; Doney et al., 2009, 2020; Gattuso et al., 2015). With atmospheric  $CO_2$  concentrations, surface ocean  
69 temperature and ocean heat content, sea-level, sea-ice and glaciers, the ocean acidification (decrease of pH) is  
70 now recognized by the World Meteorological Organization as one of the 7 key properties for global climate  
71 indicators (WMO, 2018). Ocean acidification is specifically referred in the SDG indicator 14.3.1 coordinated at  
72 the Intergovernmental Oceanographic Commission (IOC) of UNESCO. Observing the carbonate system in the  
73 open oceans, coastal zones and marginal seas and understanding how this system changes over time is thus  
74 highly relevant not only to quantify the global ocean carbon budget, the anthropogenic  $CO_2$  inventories or ocean  
75 acidification rates, but also to understand and simulate the processes that govern the complex  $CO_2$  cycle in the  
76 ocean (e.g. Goyet et al, 2016, 2019) and to better predict the future evolution of climate and global changes  
77 (Eyring et al., 2016; Kwiatkowski et al., 2020; Jiang et al., 2023). As the rate of change in ocean acidification  
78 presents large temporal and regional variability, long-term observations are required. Weekly to monthly regular  
79 resolution data are needed to better investigate the long-term change of the carbonate system in regions subject  
80 to extreme events (e.g. tropical cyclones, marine heat or cold waves, rapid freshening, convection, dust events,  
81 river discharges, etc....). In this context it is recommended to progress in data synthesis of the ocean carbon  
82 observations that would offer new high quality products for the community (e.g. for GOA-ON, [www.goa-on.org](http://www.goa-on.org),  
83 IOC/SDG 14.1.3, <https://oa.iode.org/>, Tilbrook et al., 2019).

84 In this work, following the first SNAPO- $CO_2$  synthesis product (Metzl et al, 2024a), we present a new  
85 synthesis of more than 67000  $A_T$  and  $C_T$  data, measured either on shore or onboard Research Vessels obtained  
86 over the 1993-2023 period during various cruises or at time-series stations mainly supported by French projects.  
87 Hereafter this new dataset will be cited as SNAPO- $CO_2$ -v2. The methods, data assemblage and quality control

88 were presented in version V1. Here, we describe the new data added and discuss some potential uses of this  
89 dataset.

90

## 91 2 Data collections

92

93 The time series projects and research cruises from which new data were collated are listed in Table 1  
94 with information and references in the Supplementary file (Tables S1, S3 and S4). The sampling locations of  
95 new data are displayed in Figure 1 (the location for all data presented in Figure S1). Sampling was performed  
96 either from CTD-Rosette casts (Niskin bottles) or from the ship's seawater supply (intake at about 5m depth  
97 depending on the ship and swell). Samples collected in 500 mL borosilicate glass bottles were poisoned with 100  
98 to 300  $\mu\text{L}$  of  $\text{HgCl}_2$  depending on the cruises, closed with greased stoppers (Apiezon®) and held tight using  
99 elastic band following the SOP protocol (DOE, 1994; Dickson et al., 2007). Some samples were also collected in  
100 500 mL bottles closed with screw caps. After completion of each cruise, most of discrete samples were returned  
101 back to the LOCEAN laboratory (Paris, France) and stored in a dark room at 4 °C before analysis generally  
102 within 2-3 months after sampling (sometimes within a week). In this version we added data from samples that  
103 were also returned to University of Perpignan or to University of La Réunion. In addition to discrete samples  
104 analyzed for various projects conducted mainly in the North Atlantic, Tropical Atlantic, Mediterranean Sea and  
105 coastal regions (Table 1), we complemented this second synthesis with  $A_T$  and  $C_T$  surface observations obtained  
106 in the Indian and Southern oceans during the OISO cruises in 2019-2021 (Leseurre et al., 2022; Metzl et al,  
107 2022; data also available at NCEI/OCADS: [www.nodc.noaa.gov/ocads/oceans/VOS\\_Program/OISO.html](http://www.nodc.noaa.gov/ocads/oceans/VOS_Program/OISO.html)) and  
108 MINERVE cruises in 2002-2018 (Laika et al, 2009; Brandon et al, 2022). The  $A_T$  and  $C_T$  measurements from the  
109 MINERVE cruises were performed either onboard R/V Astrolabe or back in the laboratories (at LOCEAN  
110 laboratory and at University of Perpignan).

111

112

113

114

115

116

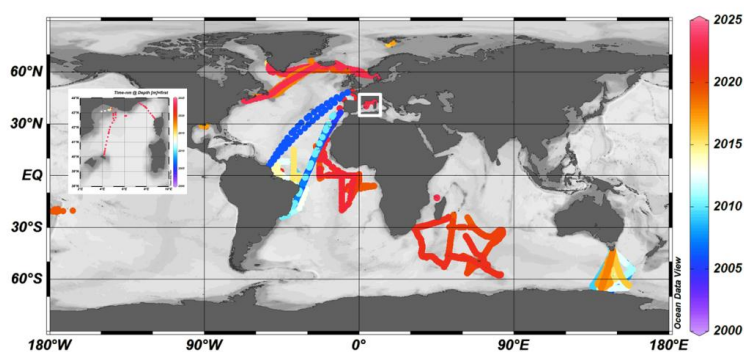
117

118

119

120

121



122 **Figure 1:** Locations of new  $A_T$  and  $C_T$  data (2005-2023) in the Global Ocean and the Western Mediterranean Sea  
123 (white box, insert) in the SNAPO-CO2-v2 dataset. Color code is for Year. Figure produced with ODV (Schlitzer,  
124 2018).

125

126 **Table 1:** List of cruises added in the SNAPO-CO2-v2 dataset. This is organized by region from North to South  
 127 and the Mediterranean Sea. See Tables S1, S2, S3 and S4 in the Supplementary Material for a list of laboratories,  
 128 of CRMs used, for DOI and for references of cruises. Nb = the number of data for each cruise or time-series. \*  
 129 indicates the measurements at sea (surface underway).

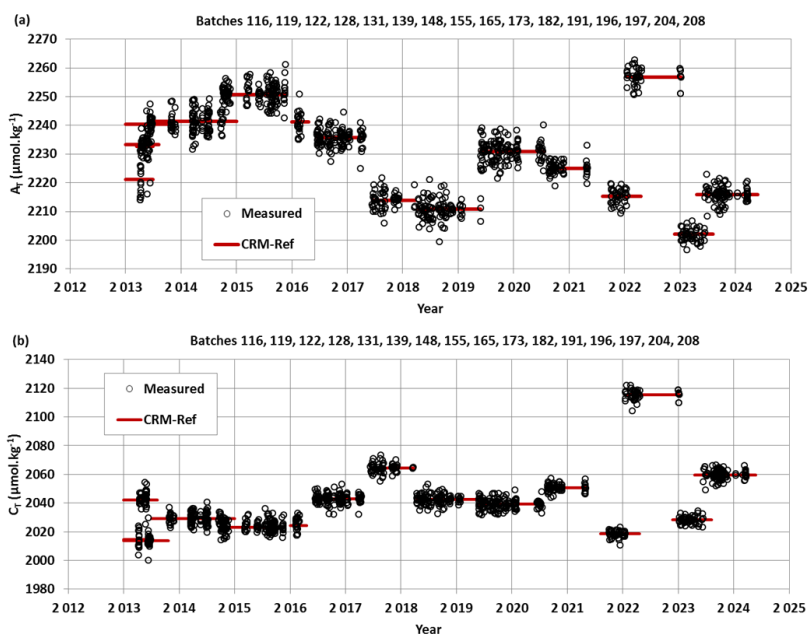
Cruise/Project	Start	End	Region	Sampling	Nb
135 STEP	2016	2017	Arctic	Water Column	33
136 SURATLANT AX1	2017	2023	North Atlantic	Surface	255
137 SURATLANT AX2	2018	2023	North Atlantic	Surface	224
138 VOS	2005	2010	Atlantic	Surface	192
139 MISSRHODIA-1	2017	2017	Gulf Mexico	Water Column	8
140 ACIDHYPO	2022	2022	Gulf Mexico	Water Column	10
141 CAMFIN-WATL	2010	2015	Trop Atlantic	Surface	192
142 PIRATA-BR	2009	2015	Trop Atlantic	Surface	194
143 BIOAMAZON	2013	2014	Trop Atlantic	Surface	62
144 AMAZOMIX	2021	2021	Trop Atlantic	Water Column	180
145 PIRATA-FR	2019	2019	Trop Atlantic	Surface	93
146 PIRATA-FR	2020	2020	Trop Atlantic	Surface, Water Column	58
147 PIRATA-FR	2021	2021	Trop Atlantic	Surface, Water Column	79
148 PIRATA-FR	2022	2022	Trop Atlantic	Surface, Water Column	118
149 CO2ARVOR	2009	2010	Atlantic, Coastal	Surface, Water Column	621
150 SOMLIT-Roscoff	2020	2022	Coastal North Atl	Surface and 60m	207
151 SOMLIT-Brest	2020	2022	Coastal North Atl	Surface	251
152 TONGA	2019	2019	Trop Pacific	Water Column	226
153 CARBODISS	2018	2019	Indian Mayotte	Surface	85
154 OISO *	2019	2021	South Indian	Surface	5258
155 MINERVE	2004	2018	Southern Ocean	Surface	1077
156 MINERVE *	2002	2013	Southern Ocean	Surface	11258
157 COCORICO2	2017	2022	Coastal	Surface	589
158 SOMLIT-PointB	2019	2023	MedSea Coastal	Surface and 50m	716
159 SOLEMIO	2018	2022	MedSea Coastal	Water Column	271
160 ANTARES	2017	2023	MedSea	Water Column	506
161 MOLA	2018	2023	MedSea Coastal	Water Column	193
162 DYFAMED	2018	2023	MedSea	Water Column	514
163 MESURHO-BENT	2010	2011	MedSea Coastal	Surface and sub-surface	25
164 ACCESS-01	2012	2012	MedSea Coastal	Water Column	16
165 CARBO-DELTA-2	2013	2013	MedSea Coastal	Water Column	14
166 DICASE	2014	2014	MedSea Coastal	Water Column	22
167 MISSRHODIA-2	2018	2018	MedSea Coastal	Surface and sub-surface	13
168 DELTARHONE1	2022	2022	MedSea Coastal	Water Column	9
169 MOOSE-GE	2021	2021	MedSea	Water Column	451
170 MOOSE-GE	2022	2022	MedSea	Water Column	447
171 MOOSE-GE	2023	2023	MedSea	Water Column	475

### 174 3 Method, accuracy, repeatability and quality control

#### 175 176 3.1 Method and accuracy

177  
 178 Since 2003, the discrete samples returned back at SNAPO-CO2 Service facilities (LOCEAN, Paris),  
 179 were analyzed simultaneously for  $A_T$  and  $C_T$  by potentiometric titration using a closed cell (Edmond, 1970;  
 180 Goyet et al., 1991). The same technique was used at sea for surface water underway measurements during OISO  
 181 and MINERVE cruises (indicated by \* in Table 1). In the late 1980s the so-called “JGOFS-IOC Advisory Panel  
 182 on Ocean CO2” recommended the need for standard analysis protocols and for developing Certified Reference  
 183 Materials (CRMs) for inorganic carbon measurements (Poisson et al., 1990; UNESCO, 1990, 1991). The CRMs

184 were provided to international laboratories by Pr. A. Dickson (Scripps Institution of Oceanography, San Diego,  
 185 USA), starting in 1990 for  $C_T$  and 1996 for  $A_T$ , respectively. These CRMs were thus always available to us and  
 186 used to calibrate the measurements (CRM Batch numbers used for each cruise are listed in the Supplementary  
 187 file, Table S2). The CRMs accuracy, as indicated in the certificate for each Batch, is around  $\pm 0.5 \mu\text{mol kg}^{-1}$  for  
 188 both  $A_T$  and  $C_T$  ([www.nodc.noaa.gov/ocads/oceans/Dickson\\_CRM/batches.html](http://www.nodc.noaa.gov/ocads/oceans/Dickson_CRM/batches.html)). The concentrations of CRMs  
 189 we used vary between 2193 and 2426  $\mu\text{mol kg}^{-1}$  for  $A_T$  and between 1968 and 2115  $\mu\text{mol kg}^{-1}$  for  $C_T$   
 190 corresponding to the range of concentrations observed in open ocean water. In the Mediterranean Sea the  
 191 concentrations are higher ( $A_T > 2600 \mu\text{mol kg}^{-1}$  and  $C_T > 2300 \mu\text{mol kg}^{-1}$ ) and in the coastal zones or near the  
 192 Amazon River plume the concentrations were often lower than the CRMs ( $A_T < 1500 \mu\text{mol kg}^{-1}$  and  $C_T < 1000$   
 193  $\mu\text{mol kg}^{-1}$ ). Results of analyses performed on 1242 CRM bottles (different Batches) in 2013-2024 are presented  
 194 in Figure 2. The standard-deviations (Std) of the differences of measurements were on average  $\pm 2.69 \mu\text{mol kg}^{-1}$   
 195 for  $A_T$  and  $\pm 2.88 \mu\text{mol kg}^{-1}$  for  $C_T$ . For unknown reasons, the differences were occasionally up to 10-15  $\mu\text{mol kg}^{-1}$   
 196 <sup>1</sup> (1.2% of the data, Figure S2). These few CRM measurements were discarded for the data processing. We did  
 197 not detect any specific signal for CRM analyses (e.g., larger uncertainty depending on the Batch number or  
 198 temporal drifts during analyses, Figure 2) but for some cruises the accuracy based on CRMs could be better than  
 199  $3 \mu\text{mol kg}^{-1}$  (e.g.  $< 3 \mu\text{mol kg}^{-1}$  for AMAZOMIX cruise using 6 Batches #197 and for MOOSE-GE 2022 using  
 200 19 Batches #204, or  $< 1.5 \mu\text{mol kg}^{-1}$  for SOMLIT-Point-B in 2022 using 6 Batches #204).



221 **Figure 2:**  $A_T$  (a) and  $C_T$  (b) analyses for different CRM Batches measured in 2013-2024. For these 1242  
 222 analyses the mean and standard-deviations of the differences with the CRM reference were  $-0.11 (\pm 2.69) \mu\text{mol}$   
 223  $\text{kg}^{-1}$  for  $A_T$  and  $0.01 (\pm 2.88) \mu\text{mol kg}^{-1}$  for  $C_T$ .

227 **3.2 Repeatability**

228

229

230

231

232

233

234

235

236

237

238

239

240

241

242

243

244

245

246

247

248

249

250

251

252

253

254

255

256

257

258

259

260

261

262

263

264

265

266

267

268

269

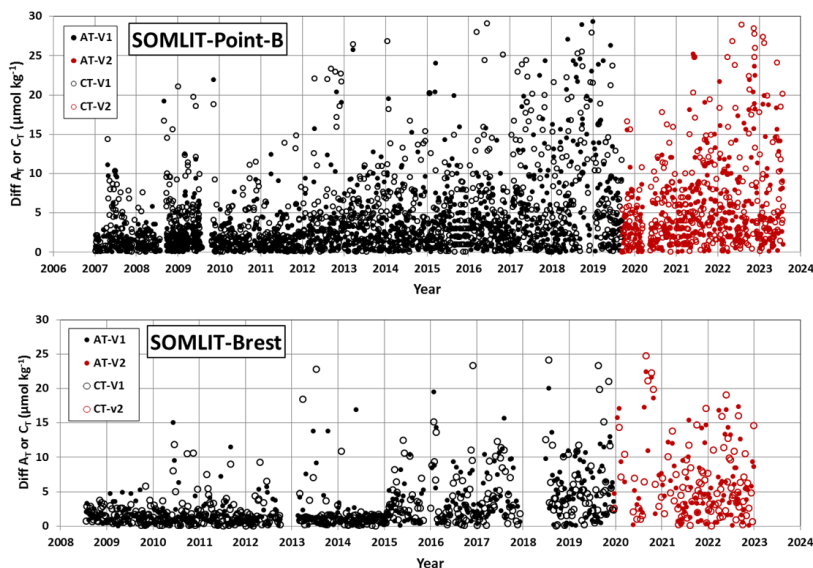


**Figure 3:** Results of duplicate  $A_T$  and  $C_T$  analyses from the time-series SOMLIT-Point-B in the coastal Mediterranean Sea and SOMLIT-Brest in the coastal Brittany for the data in the SNAPO-CO2-v1 dataset (black) and new data added in SNAPO-CO2-v2 (red). The plots show differences in duplicates for both  $A_T$  (filled circles) and  $C_T$  (open circles). Standard-deviations of these duplicates are listed in Table 2.

270 **Table 2:** Repeatability of  $A_T$  and  $C_T$  analyses for cruises with duplicate analysis. The results are expressed as the  
 271 standard-deviations (Std) of the analysis of replicated samples. Nb = the number of replicates for each Time-  
 272 series or Cruise. For the OISO cruises the mean repeatability was obtained from measurements at the same  
 273 location (when the ship stopped).

Cruise	Period	Nb	Std $A_T$ $\mu\text{mol kg}^{-1}$	Std $C_T$ $\mu\text{mol kg}^{-1}$	Reference
STEP	2017	3	0.7	2.8	Unpublished
CARBODISS	2018	10	6.72	5.71	Unpublished
SOMLIT-Point-B	2007-2019	1130	4.5	5.1	SNAPO-CO2-v1, (a)
SOMLIT-Point-B	2019-2023	321	5.2	6.2	SNAPO-CO2-v2, (a)
SOMLIT-Brest	2008-2018	404	3.1	3.4	SNAPO-CO2-v1, (a)
SOMLIT-Brest	2019-2022	142	6.0	6.1	SNAPO-CO2-v2, (a)
OISO 29	2019	46	1.8	1.8	Leseurre et al (2022), (b)
OISO 30	2020	67	1.5	2.0	Metzl et al. (2022), (b)
OISO 31	2021	343	2.6	3.3	Metzl et al (2024c), (b)

292 (a) See Figure 3 for the results of regular duplicates for time-series SOMLIT-Point-B, SOMLIT-Brest.

293 (b) Metadata and data available at [www.nodc.noaa.gov/ocads/oceans/VOS\\_Program/OISO.html](http://www.nodc.noaa.gov/ocads/oceans/VOS_Program/OISO.html)

294

295

296

### 3.3 Assigned flags for quality control

297

298

299

300

301

302

303

304

305

306

307

308

309

310

311

312

313

314

315

316

317

318

Identifying each data with an appropriate flag is very convenient for selecting the data (good, questionable or bad). Here we used 4 flags for each property (flags 2 = good, 3= questionable, 4=bad, and 9= no data) following the WOCE program and used in other data products such as SOCAT (Bakker et al., 2016) or GLODAP (Olsen et al., 2016; Lauvset et al., 2024). During the data-processing, we first assigned a flag for each  $A_T$  and  $C_T$  data based on the standard error in the calculation of  $A_T$  and  $C_T$  concentrations (non-linear regression, Dickson et al. 2007). By default, if the standard deviation on the regression is  $> 1 \mu\text{mol kg}^{-1}$ , we assigned a flag 3 (questionable) although the data could be acceptable and then used for interpretations. Flag 3 was also assigned when salinity was doubtful or when differences of duplicates were large (e.g.  $\pm 20 \mu\text{mol kg}^{-1}$ ). Flags 4 (bad or certainly bad) were assigned when clear anomalies were detected for unknown reasons (e.g. a sample probably not fixed with  $\text{HgCl}_2$  or analysis performed late during the COVID issue). A secondary quality control was performed by the PIs of each project based on data inspection, duplicates,  $A_T$ /Salinity relationship, or the mean observations in deep layers where large variability in  $A_T$  and  $C_T$  is unlikely to occur from year to year.

An example for quality flag is presented for all data from the MINERVE cruises conducted in 2002-2018 in the Southern Ocean where clear outliers have been identified (Figure S3). For the MINERVE cruises in 2002-2018 and a total of 12335  $A_T$  and  $C_T$  analyses, 24 were identified as bad (flag 4), 978 for  $A_T$  and 971 for  $C_T$  listed as questionable (flag 3), and all others are considered as good data (flag 2, i.e. about 92%). For the MOOSE-GE cruises in 2021, 2022 and 2023 (new data in SNAPO-CO2-v2) and a total of 1373  $A_T$  and  $C_T$  analyses, 2 were identified flagged as bad (flag 4), 38 for  $A_T$  and 33 for  $C_T$  listed as questionable (flag 3) all others were considered as good data (flag 2, i.e. 97%). This is better than the statistics we evaluated for the SNAPO-CO2-v1 dataset (90% flag 2 for MOOSE-GE in 2010-2019). A similar control was performed for each project.

### 319 3.4 Inter-comparisons

320

321 Inter-comparisons of measurements performed for different cruises or with different techniques help to  
322 evaluate the quality of the data and detect potential biases when merging the data in the same region obtained by  
323 different laboratories at different periods. This is especially important to interpret long-term trends of  $A_T$  and  $C_T$   
324 as well as for  $p\text{CO}_2$  and pH calculated with  $A_T$   $C_T$  pairs. The synthesis of various cruises in the same region and  
325 periods also offers verification and secondary control of the data.

326

#### 327 3.4.1 Comparisons in deep layers

328

329 Comparisons of data in the deep layers from different cruises are useful for secondary quality control as  
330 one expects low natural variability or anthropogenic signals from season to season and over a few years. Several  
331 cruises were conducted in the Mediterranean Sea in 2017-2023 (MOOSE-GE, ANTARES and DYFAMED). The  
332 mean values of  $C_T$  and  $A_T$  in the deep layers (> 1800m) for each cruise confirmed the coherence of the data  
333 (Table 4). The  $C_T$  and  $A_T$  concentrations are also in the range of the mean values evaluated for cruises conducted  
334 in 2014 in the Mediterranean Sea (results listed in the SNAPO-CO<sub>2</sub>-v1 synthesis, Metzl et al, 2024a). In the  
335 western tropical Pacific we also observed coherent properties for the TONGA and OUTPACE cruises (Wagener  
336 et al, 2018) for data selected at 1800-2300m layer corresponding to the  $C_T$  maximum layer in the Pacific Deep  
337 Water (PDW). On the other hand in the western tropical Atlantic near the Amazon River plume where the spatial  
338 variability of the properties is large at the surface (Ternon et al, 2000; Mu et al, 2021; Olivier et al, 2022) the  
339 comparison in the water column is less clear (Figure S4). Nevertheless for the AMAZOMIX and the TARA-  
340 Microbiome cruises, both conducted in September 2021, the results at close stations (around 5°N/50°W) suggest  
341 very similar concentrations at 1000m (Table 4). The comparisons in deep waters enabled to merge the different  
342 datasets for interpretations of the temporal trends and processes driving the CO<sub>2</sub> cycle in these regions (e. g.  
343 Ulses et al., 2023 and Wimart-Rousseau et al., 2023 for the Mediterranean Sea)

344

#### 345 3.4.2 Comparing on board and on shore results

346

347 In surface waters where the variability is high inter-comparison is not relevant for secondary quality  
348 control. However, during the MINERVE cruises, discrete samples were occasionally performed along with sea  
349 surface underway measurements. Thus, we can compare  $A_T$  and  $C_T$  measured in the laboratory with those  
350 measured onboard as described by Laika et al. (2009) for the MINERVE cruises in 2005-2006. It should be  
351 noticed that the discrete samples were measured after a long trip (shipping boxes from Hobart, Tasmania to  
352 Paris, France) and thus generally analyzed at least 3 months after the cruises (cruises conducted in October to  
353 February, analyses performed in May-June). Given all the uncertainties associated to the sampling, samples  
354 storage and transport, analyses and CRMs, the mean differences between discrete and underway data are still  
355 reasonable (Std ranging between 4 and 12  $\mu\text{mol kg}^{-1}$ , Table 5). For unknown reasons the mean difference was  
356 high for a cruise in 2008-2009 (Std > 10  $\mu\text{mol kg}^{-1}$ , the “weather goal”, Newton et al., 2015). With this in mind,  
357 we believe the MINERVE data (both underway and discrete data) are useful to interpret the change of properties  
358 in this region at seasonal or decadal scales (Laika et al., 2009; Brandon et al., 2022).

359



360 **Table 4:** Mean observations in the deep layers (> 1800m) of the Ligurian Sea (Western Mediterranean Sea for  
361 different cruises conducted in 2017-2023), of the Tropical Pacific (around 2000m for cruises in 2017 and 2019),  
362 and of the Tropical Atlantic (around 1000m for cruises in 2021).  $N-A_T$  and  $N-C_T$  are  $A_T$  and  $C_T$  normalized at  
363 salinity ( $S = 38$  in the Ligurian Sea;  $S = 35$  for the Pacific and the Atlantic Oceans). Nb = number of data (with  
364 flag 2). Standard deviations are in brackets.

Cruise	Period	Nb	Pot. Temp (°C)	Salinity	$N-A_T$ ( $\mu\text{mol kg}^{-1}$ )	$N-C_T$ ( $\mu\text{mol kg}^{-1}$ )
Ligurian Sea (> 1800m)						
All Cruises	2017-2023	227	12.923 (0.052)	38.484 (0.003)	2558.3 (10.5)	2300.0 (10.7)
DYFAMED	2017-2022	74	12.913 (0.006)	38.485 (0.002)	2555.1 (11.8)	2297.3 (12.4)
ANTARES	2017-2023	62	12.944 (0.096)	38.485 (0.005)	2559.8 (9.0)	2302.2 (8.9)
MOOSE-GE	2017-2023	91	12.917 (0.005)	38.484 (0.003)	2559.8 (9.8)	2300.7 (10.0)
Tropical Pacific (layer 1800-2300m)						
OUTPACE	2017	15	2.124 (0.055)	34.633 (0.006)	2414.1 (8.0)	2318.8 (5.8)
TONGA	2019	7	2.196 (0.197)	34.619 (0.016)	2408.9 (9.1)	2327.2 (7.5)
Western Tropical Atlantic (1000m)						
AMAZOMIX	2021	14	4.770 (0.105)	34.711 (0.041)	2315.6 (20.2)	2220.8 (17.1)
TARA-MICRO	2021	1	4.852	34.717	2312.9	2231.1

403 **Table 5:** Comparison of  $A_T$  and  $C_T$  analysed on-board and at SNAPO-CO2 facilities for the MINERVE project.  
404 The results are expressed as the standard deviations (Std) of the differences for each cruise. Nb = the number of  
405 co-located samples.

Period	Nb	Std $A_T$ $\mu\text{mol kg}^{-1}$	Std $C_T$ $\mu\text{mol kg}^{-1}$
2004-2005	109	12.85	4.99
2005-2006	45	4.20	6.77
2007-2008	17	10.15	10.62
2008-2009	26	15.80	12.02
2009-2010	22	4.04	5.78
2010-2011	33	9.36	6.83
2012-2013	29	5.43	9.73

422 **3.4.3 Comparison based on different techniques**

423

424

425

426

427

428

429

430

431

432

433

434

435

436

437

438

439

440

441

442

443

444

445

446

447

448

449

450

451

452

453

454

455

456

457

458

459

460

461

462

463

464

Another example of comparison is presented for samples obtained in the lagoon of Mayotte Island in the western Indian Ocean and measured using different techniques. In the frame of the CARBODISS project seawater was sampled in 2018-2023 at several coral reef sites within the north-eastern part of the lagoon and measured either at LOCEAN laboratory or at La Réunion University. To remove coral sand particles the water samples were immediately filtered through Whatman GF/F filters and poisoned with mercuric chloride, following Dickson et al. (2007). In 2021, 2022 and 2023,  $A_T$  was measured at La Réunion University using an automated potentiometric titration (905 Titrande Metrohm titrator with combined pH electrode 6.0253.00) and calculated from the second inflection point of the titration curve. The HCl concentration was checked each day of measurements using a CRM provided by A. Dickson, Scripps Institution of Oceanography. The  $A_T$  precision of  $\pm 2 \mu\text{mol kg}^{-1}$  was based on triplicate ~~was estimated  $\pm 2 \mu\text{mol kg}^{-1}$  analyses~~ (Lagoutte et al., 2023). In the studied coral reef sites  $A_T$  concentrations ranged between 2250 and 2350  $\mu\text{mol kg}^{-1}$  but with occasional higher concentrations up to 2450-2500  $\mu\text{mol kg}^{-1}$ . Such high  $A_T$  has been observed in other coral reefs ecosystems (Cyronak et al., 2013 at Cook Island; Palacio-Castro et al., 2023 at Middle Keys, Florida). The data obtained in the lagoon of Mayotte on different coral reefs could be compared with underway observations obtained offshore of Mayotte Island (OISO-11 cruises in 2004 and CLIM-EPARSEES cruise in 2019, data available in the SNAPO-CO2-v1 dataset). In the open ocean the  $A_T$  concentrations ranged between 2250 and 2330  $\mu\text{mol kg}^{-1}$ , close to the results obtained at Mayotte reefs except for samples in November 2021 that were all collected at Cratère station (12.84°S-45.39°E) (Figure 4). At this location there was a large diurnal variation in November 2021 with  $A_T$  increasing from 2322 to 2508  $\mu\text{mol kg}^{-1}$  (Figure S5). This is because in 2021 the samples were taken at low tide recording a volcanic signal at this site allowing recording for the first time the volcanic signal in this location ( $\text{CO}_2$  resurgences). In 2018 and 2019 such high  $A_T$  were not measured (Figure S5) as samples were taken at high tides allowing a certain dilution of volcanic  $\text{CO}_2$  emissions in the water column. Although the samples were measured with different techniques the range of  $A_T$  is coherent for both datasets (Figure 4). Therefore we added the  $A_T$  data measured at La Réunion University in 2021-2023 to complete the synthesis for this location (Mayotte Island).

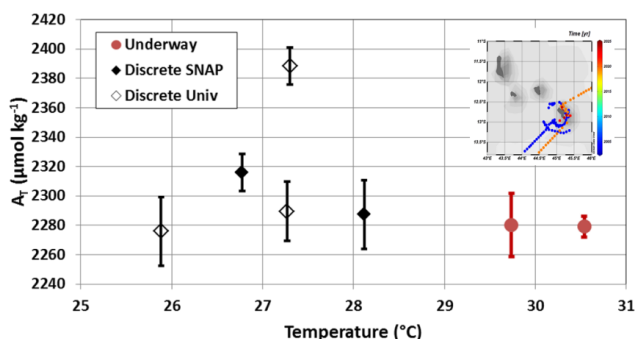


**Figure 4:** Total alkalinity ( $A_T$ ) versus temperature for samples measured around Mayotte and in the coral reef (insert map). Underway  $A_T$  was measured onboard in 2004 and 2019 (red circles) whereas discrete samples at different reef sites within the lagoon of Mayotte in 2018, 2019, 2021, 2022 and 2023 were measured at

465 LOCEAN (black diamonds) or at La Réunion University (open diamonds). The figure presents the data averaged  
 466 for each cruise in this region.

467

### 468 3.4.4 Summary of quality control data

469

470 The total number of data in the SNAPO-CO2-v2 dataset for the Global Ocean is gathered in Table 6  
 471 with corresponding flags for each property. Overall, the synthesis includes more than 91% of good data for both  
 472  $A_T$  and  $C_T$ . About 6% are questionable and 3% are likely bad. Overall, we believe that all data (with flag 2) in  
 473 this synthesis have an accuracy better than  $4 \mu\text{mol kg}^{-1}$  for both  $A_T$  and  $C_T$ , the same as for quality-controlled  
 474 data in GLODAP (Lauvset et al., 2024). The uncertainty ranges between the “Climate goal” ( $2 \mu\text{mol kg}^{-1}$ ) and  
 475 the “Weather Goal” ( $10 \mu\text{mol kg}^{-1}$ ) for ocean acidification studies (Newton et al., 2015; Tilbrook et al., 2019).  
 476 This accuracy is also relevant to validate or constraint data-based methods that reconstruct  $A_T$  and  $C_T$  fields with  
 477 an error of around  $10\text{-}15 \mu\text{mol kg}^{-1}$  for both properties (Bittig et al., 2018; Broullón et al., 2019, 2020; Fourier et  
 478 al., 2020; Gregor and Gruber, 2021; Chau et al., 2024a).

479

480

481 **Table 6:** Number of Temperature, Salinity,  $A_T$  and  $C_T$  data in the SNAPO-CO2-v2 synthesis identified for flags  
 482 2 (good), 3 (questionable), 4 (bad), 9 (no data). Last column is the percentage of flag 2 (Good).

483

484

Property	Flag 2	Flag 3	Flag 4	Flag 9	% flag 2
Temperature	68253	418	0	653	99.4
Salinity	68706	482	5	131	99.3
$A_T$	61249	3910	2077	2088	91.1
$C_T$	61869	3865	2057	1533	91.3

492

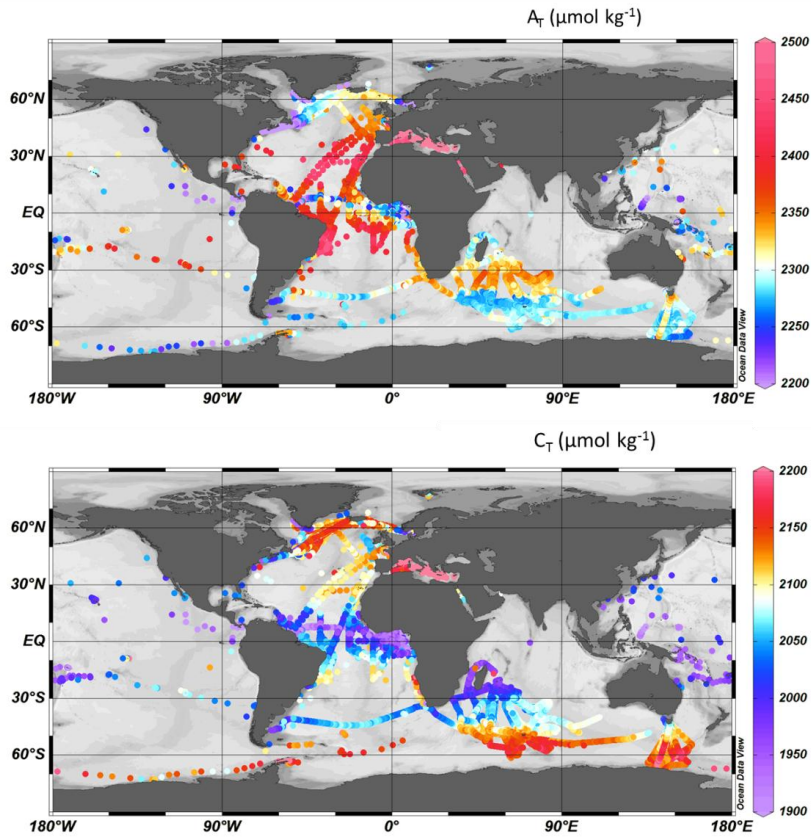
493

### 494 4 Global $A_T$ and $C_T$ distribution based on the SNAPO-CO2-v2 dataset

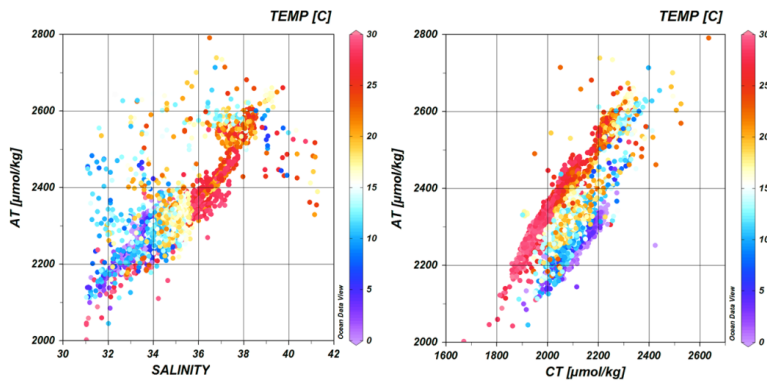
495

496 The surface distribution in the global ocean based on the SNAPO-CO2 dataset is presented in Figure 5  
 497 for  $A_T$  and  $C_T$ . The  $A_T$ /Salinity and  $A_T$ / $C_T$  relationships are clearly identified and structured at regional scale  
 498 (Figure 6). In the open ocean, high  $A_T$  concentrations ( $> 2400 \mu\text{mol kg}^{-1}$ ) are identified in the Atlantic subtropics  
 499 (bands  $35^\circ\text{N}\text{-}15^\circ\text{N}$  and  $25^\circ\text{S}\text{-}3^\circ\text{S}$ ) (Jiang et al., 2014; Takahashi et al., 2014). The lowest  $A_T$  and  $C_T$   
 500 concentrations ( $< 600 \mu\text{mol kg}^{-1}$ ) are observed in the western tropical Atlantic in the Amazon River plume near  
 501 the mouth (Lefèvre et al., 2017b). For  $C_T$  the concentrations are high ( $> 2150 \mu\text{mol kg}^{-1}$ ) in the Southern Ocean  
 502 south of the polar front, associated with the deep mixing in winter and the upwelling of deep water (Metzl et al.,  
 503 2006; Pardo et al., 2017). The highest  $C_T$  concentrations (up to  $2180\text{-}2270 \mu\text{mol kg}^{-1}$ ) are observed in the high  
 504 latitudes of the Southern Ocean near the Adélie coastal zone (MINERVE and ACE cruises), around the  
 505 Kerguelen plateau (OISO-31 cruise) and close to the Antarctic Peninsula (TARA-Microbiome cruise). In the  
 506 North Atlantic the new data from SURATLANT cruises in 2018-2023 confirm the high  $C_T$  concentrations ( $>$   
 507  $2150 \mu\text{mol kg}^{-1}$ ) observed in the Sub-polar gyre since 2016 due in part to the accumulation of anthropogenic  $\text{CO}_2$   
 508 (Leseurre et al., 2020). Low  $C_T$  concentration ( $< 2000 \mu\text{mol kg}^{-1}$ ) are found in the tropics ( $10^\circ\text{N}\text{-}30^\circ\text{S}$ ) with  
 509 lower values ( $< 1950 \mu\text{mol kg}^{-1}$ ) in the equatorial Atlantic band  $10^\circ\text{N}\text{-Eq}$  (e.g. Koffi et al., 2010; Lefèvre et al.,

510 2021). In the Amazon shelf sector  $C_T$  can reach even lower concentration ( $< 1700 \mu\text{mol kg}^{-1}$ , AMAZOMIX  
 511 cruise).



525  
 526  
 527  
 528  
 529  
 530  
 531  
 532  
 533  
 534  
 535  
 536  
 537  
 538  
 539  
 540  
 541 **Figure 5:** Distribution of  $A_T$  (top) and  $C_T$  (bottom) concentrations ( $\mu\text{mol.kg}^{-1}$ ) in surface waters (0-10m) in the  
 542 SNAPO-CO2-v2 dataset. Only data with flag 2 are presented in these figures. Figures produced with ODV  
 543 (Schlitzer, 2018).



544  
 545  
 546  
 547  
 548  
 549  
 550  
 551  
 552  
 553  
 554  
 555  
 556  
 557  
 558  
 559  
 560  
 561  
 562 **Figure 6:** Relationships between  $A_T$  and Salinity (left panel) and  $A_T$  versus  $C_T$  (right panel) for samples in  
 563 surface waters (0-10m and Salinity  $> 31$ ). Only data with flag 2 are presented (nb = 48749). The color scales

564 correspond to the temperature. The data not aligned correspond to coastal zones (e.g. COCORICO2 stations).  
565 Figures produced with ODV (Schlitzer, 2018).

Mis en forme : Police :Times New Roman, Anglais (États Unis)

## 567 5 Regional $A_T$ and $C_T$ distributions and trends based on the SNAPO-CO2 dataset

568

569 The regional distributions are described for the Mediterranean Sea and for selected regions in the open  
570 ocean and coastal zones where the data are available for 10 years or more to explore the  $A_T$  and  $C_T$  trends. Given  
571 the observed seasonal and inter-annual variability and that the time-series were not regular (e.g. at monthly  
572 frequency), we cannot use recommended methods to estimate the trends (e.g. based on de-seasoned data, Sutton  
573 et al., 2022). Here we have selected the locations and seasons where the  $C_T$  trends can be linearly fitted and  
574 compared with no interpolation to fill gaps and discontinuous data (e.g., fewer samples during the COVID  
575 period).

576

### 577 5.1 The Mediterranean Sea

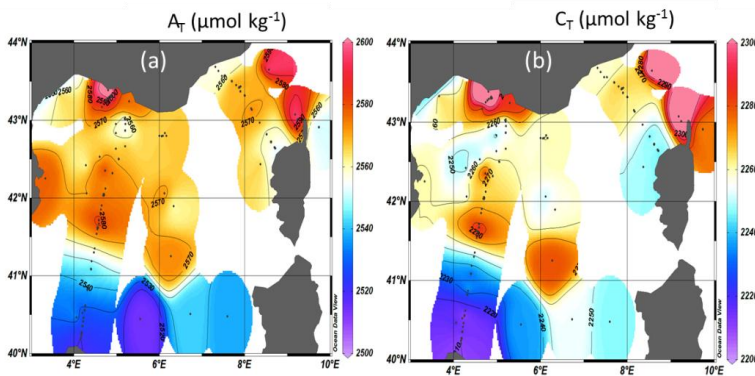
578

579 Compared to the open ocean,  $A_T$  concentrations are much higher in the Mediterranean Sea (Copin-  
580 Montégut, 1993; Schneider et al., 2007; Álvarez et al., 2023) with values up to 2600  $\mu\text{mol kg}^{-1}$ . The  $A_T$  and  $C_T$   
581 data obtained in 2014-2023 show a clear contrast between the northern and southern regions of the Western  
582 Mediterranean Sea with higher concentration in the Ligurian Sea and the Gulf of Lion (Figure 7). This contrast is  
583 associated to the circulation and the frontal system in this region (e.g. Barral et al., 2021). New data in the coastal  
584 zones in the Gulf of Lion (ACCESS, DICASE, CARBODELTA, COCORICO2, MESURHOBENT) also have  
585 very high  $A_T$  and  $C_T$  concentrations ( $A_T > 2600 \mu\text{mol kg}^{-1}$ ;  $C_T > 2350 \mu\text{mol kg}^{-1}$ ). Very low  $A_T$  and  $C_T$   
586 concentrations ( $A_T < 2500 \mu\text{mol kg}^{-1}$ ;  $C_T < 2200 \mu\text{mol kg}^{-1}$ ) were also occasionally observed in the coastal zones  
587 (COCORICO2 stations, Petton et al., 2024).

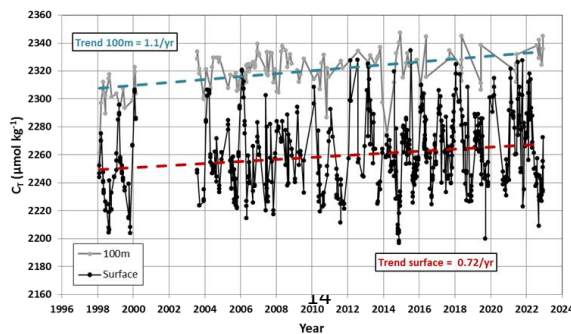
588

589 In summer 2022 the Mediterranean Sea experienced an exceptional warming (Figure S6) superposed to  
590 the long-term warming in the ocean (Cheng et al., 2024). Such event would impact the internal ocean processes  
591 such as thermodynamic, stratification and biological processes (Coppola et al., 2023) and the inter-annual  
592 variability and trends of  $C_T$ , pH,  $f\text{CO}_2$  and air-sea  $\text{CO}_2$  fluxes (Yao et al., 2016; Wimart-Rousseau et al., 2023;  
593 Chau et al., 2024b). As in 2003, the warming in summer 2022 was associated to the drought event that occurred  
594 in Europe and over the Mediterranean Sea (Faranda et al., 2023). In July 2022, the maximum temperature of  
595 28.42°C was observed at station SOMLIT-Point-B. In the Ligurian Sea the temperature trend was faster in recent  
596 years,  $+0.173 \pm 0.072 \text{ }^\circ\text{C per decade}$  over 1990-2010 and  $+0.678 \pm 0.143 \text{ per decade}$  over 2010-2023 (Figure  
597 S6). With the new data added in the SNAPO-CO2-v2 synthesis (DYFAMED, MOOSE-ANTARES, and  
598 MOOSE-GE) we evaluated a temperature trend of  $+0.84 \pm 0.20 \text{ }^\circ\text{C per decade}$  over 1998-2022 indicating that  
599 the discrete sampling captured the property changes at regional scale. Based on the data in the Ligurian Sea the  
600 trends of  $C_T$  appeared faster in summer ( $+1.53 \pm 0.46 \mu\text{mol kg}^{-1} \text{ yr}^{-1}$ ) than in winter ( $+0.94 \pm 0.64 \mu\text{mol kg}^{-1} \text{ yr}^{-1}$ ,  
601 Table 7). On the other hand, the trends of  $A_T$  were the same ( $+0.72 \pm 0.36 \mu\text{mol kg}^{-1} \text{ yr}^{-1}$  in winter and  $+0.69 \pm$   
602  $0.42 \mu\text{mol kg}^{-1} \text{ yr}^{-1}$  in summer). The trend of  $C_T$  in surface in winter was close to the one derived at 100m (below  
603 the Chl-a maximum),  $C_T^{100\text{m}} = +1.10 \pm 0.17 \mu\text{mol kg}^{-1} \text{ yr}^{-1}$  (Figure 8) whereas for  $A_T$  the trend was the same in  
604 surface and at depth ( $+0.76 \pm 0.12 \mu\text{mol kg}^{-1} \text{ yr}^{-1}$ ). This suggests that the winter  $C_T$  data recorded the  
anthropogenic  $\text{CO}_2$  uptake of around  $+1 \mu\text{mol kg}^{-1} \text{ yr}^{-1}$ , Figure S7). Note that, given the observed  $C_T$  trends, the

605 [spatial view presented in Figure 7b for 2014-2023 would be the same based on  \$C\_T\$  concentrations normalized to](#)  
 606 [a reference year \(not shown\)](#). As noted by Touratier and Goyet (2009) the  $C_T$  concentrations in the  
 607 Mediterranean Sea should increase in parallel with the level of atmospheric anthropogenic  $CO_2$ . For an  
 608 atmospheric  $CO_2$  rate of  $+2.16 \text{ ppm yr}^{-1}$  over 1998-2023 (Lan et al., 2024) and at fixed sea surface temperature  
 609 ( $17.75^\circ\text{C}$ ), salinity (38.25) and  $A_T$  ( $2567 \text{ } \mu\text{mol kg}^{-1}$ ), the theoretical  $C_T$  increase would be  $+1.24 \text{ } \mu\text{mol kg}^{-1} \text{ yr}^{-1}$ .  
 610 Interestingly, an anthropogenic flux of  $-0.3 \pm 0.02 \text{ molC m}^{-2} \text{ yr}^{-1}$  in the Mediterranean Sea (Bourgeois et al.,  
 611 2016) would correspond to an increase of  $C_T$  of  $1.07 \pm 0.07 \text{ } \mu\text{mol kg}^{-1} \text{ yr}^{-1}$  in the top 100 meters. This is again  
 612 close to what is observed in winter or at 100m (Table 7, Figure 8). On the other hand the faster  $C_T$  trend  
 613 observed in surface waters during summer might be associated with a decrease in biological production and/or  
 614 changes in circulation/mixing over time that deserve specific investigations such as analyzed for the oxygen  
 615 budget in this region (Ulses et al, 2021). It is worth noting that the  $C_T$  and  $A_T$  trends in coastal zones of the  
 616 Mediterranean Sea are opposite to those observed offshore: for example at station SOLEMIO (Bay of Marseille,  
 617 Wimart-Rousseau et al., 2020) the  $C_T$  and  $A_T$  concentrations decreased over 2016-2022 and thus opposed to the  
 618 anthropogenic  $CO_2$  signal, indicating that processes such as riverine inputs, advection or biology control the  
 619 carbonate system decadal variability at local scale. This calls for developing dedicated complex biogeochemical  
 620 models to resolve these processes (Barré et al., 2023, 2024), especially when extreme events occurred, such as  
 621 the very hot summer in 2024 with SST up to  $30^\circ\text{C}$  in the Mediterranean Sea (Platforms Buoy/Mooring AZUR,  
 622 EOL and La Revellata, data available at <https://dataselection.coriolis.eu.org/>). The data obtained in the  
 623 Mediterranean Sea are important not only to validate biogeochemical models but also to reconstruct the  
 624 carbonate system from  $A_T$  and  $pCO_2$  data (Chau et al., 2024a) as the global  $A_T$ /SSS relationships (e.g. Carter et  
 625 al., 2018) are not suitable for this region.



637 **Figure 7:** Distribution of  $A_T$  (a) and  $C_T$  (b) in  $\mu\text{mol kg}^{-1}$  in surface waters of the Mediterranean Sea (0-10m) from  
 638 observations over 2014-2023. Figures produced with ODV (Schlitzer, 2018).



649

650  
651  
652  
653  
654  
655  
656  
657

Figure 8: Time-series of  $C_T$  concentrations in surface (black symbols) and at 100m (grey symbols) in the Ligurian Sea. The trends over 1998-2022 is surface (red) and at 100m (blue) are indicated by dashed lines.

## 658 5.2 The North Atlantic

659

660 The North Atlantic Ocean is an important  $\text{CO}_2$  sink (Takahashi et al. 2009) due to biological activity  
661 during summer, heat loss and deep convection during winter. As a result this region contains high concentrations  
662 of anthropogenic  $\text{CO}_2$  ( $C_{\text{ant}}$ ) in the water column (Khaliwala et al., 2013). Decadal variations of the  $C_{\text{ant}}$   
663 inventories were recently identified at basin scale probably linked to the change of the overturning circulation  
664 (Gruber et al., 2019; Müller et al., 2023; Pérez et al., 2024). This region experienced climate modes such as the  
665 North Atlantic Oscillation (NAO) and the Atlantic Multidecadal Variability (AMV) that imprint variability in  
666 air-sea  $\text{CO}_2$  fluxes at inter-annual to multidecadal scales (e.g. Thomas et al., 2008; Jing et al., 2019;  
667 Landschützer et al., 2019) but not always clearly revealed at regional scale (Metzl et al., 2010; Schuster et al.,  
668 2013; Pérez et al., 2024). In addition it has been recently shown that extreme events such as the marine heat  
669 wave in summer 2023 led to a reduce  $\text{CO}_2$  uptake in this region (Chau et al., 2024b). Although the annual  
670  $\text{CO}_2$  fluxes deduced from Global Ocean Biogeochemical Models (GOBM) seem coherent with the data-products  
671 at basin scale (resp.  $-0.30 \pm 0.07$  and  $-0.24 \pm 0.03$  PgC/yr for the [North Atlantic subpolar seasonally stratified](#),  
672 NA-SPSS biome) the  $p\text{CO}_2$  cycle seasonality is not well simulated (Pérez et al., 2024). Therefore to correct the  
673 GOBMs outputs, comparisons with the observed  $C_T$  and  $A_T$  cycles are also needed.

674 In this context regular sampling in the North Atlantic (OVIDE cruises, Mercier et al., 2015, 2024;  
675 SURATLANT transects, Reverdin et al., 2018) and time-series stations in the Irminger and Iceland Seas  
676 (Ólafsson, et al., 2010; Lange et al., 2024; Yoder et al., 2024) are important to explore the variability of the  
677 biogeochemical properties from seasonal (Figure S8) to decadal scales (Figure 9). The SURATLANT data added  
678 in the SNAPO-CO2-v2 dataset over 2017-2023 offer new observations in the North Atlantic Subpolar Gyre  
679 (NASPG in the NA-SPSS biome) and new transects from Norway to Iceland and reaching the coast of Greenland  
680 (Figure 9). In 2010 the winter NAO was negative, moved to a positive state in 2012-2020 and was again very  
681 low in 2021. The new SURATLANT data after 2017 confirm the cooling and the freshening in the NASPG since  
682 2009 (Holliday et al., 2020; Leseurre et al., 2020; Siddiqui et al., 2024) whereas the most recent data in 2022 and  
683 2023 suggest a reverse trend (increase of salinity and temperature, not shown). After 2016, large  $C_T$  anomalies in  
684 the NASPG were observed. For examples, in April 2019 and 2022, the  $C_T$  concentrations were low compared to  
685 2016 (Figure 9) and opposed to the expected anthropogenic  $\text{CO}_2$  uptake. In September 2023 the  $C_T$   
686 concentrations were much lower than in 2022 (Figure 9) probably linked to biological productivity when the  
687 NAO index was negative (Fröb et al., 2019) as observed in summer 2023 (NAO < -2 in July 2023). Despite these  
688 variability the  $C_T$  trends are relatively well evaluated (Table 7). As in the Mediterranean Sea the  $C_T$  trends in the  
689 NASPG appeared different depending on the season (Figure 9). The  $C_T$  increase was faster in September than in  
690 April (resp.  $+1.09 \pm 0.37 \mu\text{mol kg}^{-1} \text{yr}^{-1}$  and  $+0.78 \pm 0.23 \mu\text{mol kg}^{-1} \text{yr}^{-1}$ ). This is either close to or lower than the  
691 theoretical  $C_T$  increase due to the rising of atmospheric  $\text{CO}_2$  ( $+0.91 \mu\text{mol kg}^{-1} \text{yr}^{-1}$ ) and in the range of recent

692 results evaluated for the Sub-polar Mode Waters in the Irminger Sea ( $C_{\text{ant}}$  trend =  $0.95 \pm 0.17 \mu\text{mol kg}^{-1} \text{yr}^{-1}$  for  
 693 the period 2009-2019, Curbelo-Hernández et al., 2024).

694

695

696

697

698

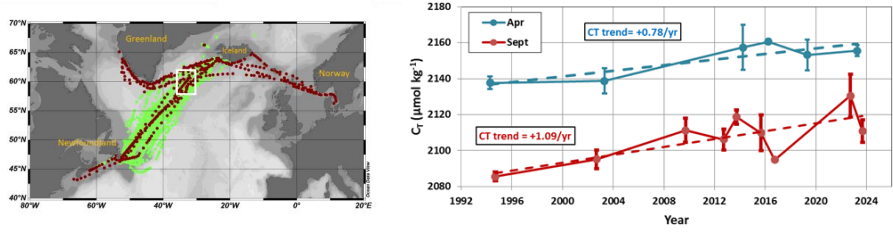
699

700

701

702

703



704 **Figure 9:** Left: Data in SNAPO-CO2-v1 (green) and new data in v2 (brown) from the SURATLANT cruises in  
 705 1993-2023 in the North Atlantic. Figure produced with ODV (Schlitzer, 2018). The white box identified the  
 706 region of selected data around 60°N for the trend analysis. Right: Time-series of average  $C_T$  concentrations in  
 707 April (blue) and September (red) in this region. The trends for each season are indicated (see also Table 7).  
 708

### 709 5.3 The Tropical Atlantic

710

711

712

713

714

715

716

717

718

719

720

721

722

723

724

725

726

727

728

729

730

731

732

733

734

735

In the Tropical Atlantic, previous studies highlighted the large variability of biogeochemistry and the difficulty in detecting long-term trends of  $C_T$  (e.g. Lefèvre et al., 2021). This is related to the variability of circulation, equatorial upwelling, biological processes (some linked to Saharan dust) and inputs from large rivers (Congo, Amazon and Orinoco). The new data added in version SNAPO-CO2-v2 (Figure S9) show the contrasting zonal  $C_T$  distribution in this region with lower concentrations in low salinity regions of the North Equatorial Counter Current and Guinea Current (Figure 5; Oudot et al., 1995; Takahashi et al., 2014; Broullón et al., 2020; Bonou et al., 2022). For exploring the temporal changes we selected the data in the western region available for at least 10 years and separated the northern and southern sectors. In both regions the  $C_T$  trend is close to  $+3 \mu\text{mol kg}^{-1} \text{yr}^{-1}$  (Table 7, Figure S9) much higher than the expected anthropogenic signal. In this region where coastal water masses mixes with oceanic waters, the inter-annual variability of  $C_T$  is large and the changes driven by competitive processes (circulation, biological processes). More observations and dedicated models are needed to separate the anthropogenic and natural variability in this region (Pérez et al., 2024).

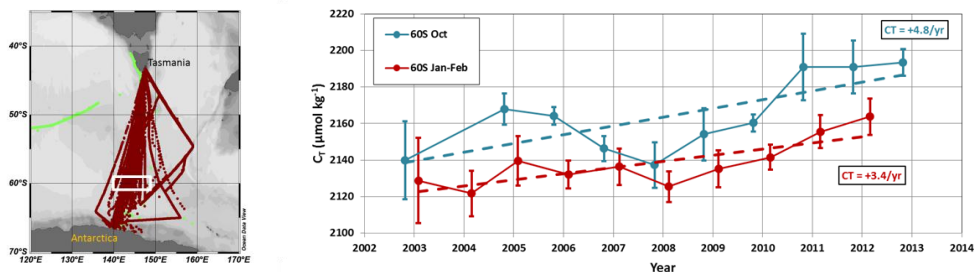
### 724 5.4 The Southern Ocean

In the Southern Ocean there are a few regular multi-annual observations of the carbonate system. Time series of more than 10 years were obtained in the Drake Passage (Munro et al., 2015) and in the Southern Indian Ocean (Leseurre et al., 2022; Metzl et al., 2024b). Observations were also obtained for more than 20 years southeast of New Zealand at the Munida Time Series (MTS) in the subtropical and sub-Antarctic frontal zones (Currie et al., 2011; Vance et al., 2024). To complement these datasets we have added the data collected in the South-Eastern Indian Ocean between Tasmania and Antarctica in the frame of the MINERVE cruises (Figure 10; Brandon et al., 2022). These cruises were conducted from October to March offering each year a view of the seasonal changes between late winter and summer from the sub-Antarctic zone to the coastal zone near Antarctica (Adélie land). In all sectors (here from 45°S to 67°S) the  $C_T$  concentrations were higher in October when the mixed-layer depth (MLD) was deep and were lower during the productive summer season (e.g. Laika



736 et al., 2009; Shadwick et al., 2015). An example is presented at 60°S/151°E from the data obtained along a  
 737 reoccupied track in 2011-2012 (Figure S10). At this location south of the Polar Front in the POOZ/HNLC area,  
 738 (Permanent Open Ocean Zone/ High Nutrient Low Chlorophyll), the  $C_T$  concentrations were  $+25 \mu\text{mol kg}^{-1}$   
 739 higher in October compared to February. The same seasonal amplitude was observed in the western Indian sector  
 740 of the POOZ (Metzl et al., 2006, 2024b) suggesting that the  $C_T$  seasonality is relatively homogeneous in this  
 741 region corresponding to the Indian SO-SPSS biome (Fay and McKinley, 2014). The difference in the  
 742 climatological  $C_T$  between October and January is on average  $+28.3 \pm 9.8 \mu\text{mol kg}^{-1}$  in the Indian Ocean POOZ  
 743 (Takahashi et al., 2014). Given this seasonality and potential change in the seasonal amplitude over time  
 744 (Gallego et al., 2018; Landschützer et al., 2018; Shadwick et al., 2023) the property trends have to be evaluated  
 745 for October and January-February separately, here over 2002-2012 in the POOZ (Figure 10, Table 7). In both  
 746 seasons, the average  $C_T$  concentrations reached a minimum in 2008 and increased faster in 2008-2012 (up to  
 747  $+4.8 \mu\text{mol kg}^{-1} \text{ yr}^{-1}$ ). Interestingly, such acceleration of the trend after 2009 was observed for  $p\text{CO}_2$  at the MTS  
 748 station (Vance et al., 2024). We note that the  $C_T$  trend over 2002-2012 was slightly faster in October (Figure 10)  
 749 probably linked to deeper MLD as suggested from the cooling and the salinity increase observed during this  
 750 season (not shown).

751  
752  
753  
754  
755  
756  
757  
758  
759  
760  
761  
762



763 **Figure 10:** Left: Data in SNAPO-CO2-v1 dataset (green) and new data in version v2 (brown) in the South  
 764 eastern Indian Ocean. Figure produced with ODV (Schlitzer, 2018). The white box identified the region of  
 765 selected data around 60°S for the trend analysis. Right: Time-series of average  $C_T$  concentrations in January-  
 766 February (red) and October (blue) around 60°S (white box in the map). The trends for each season are indicated  
 767 (see also Table 7).

768  
769 In the western Indian sector, the new data in the SNAPO-CO2-v2 dataset from the OISO cruises at high  
 770 latitudes also recorded a rapid  $C_T$  trend over 5-8 years periods (e.g.,  $+3.4 \mu\text{mol kg}^{-1} \text{ yr}^{-1}$  in 2015-2020 at 56°S,  
 771 Figure 11, Table 7). Although the inter-annual variability of  $C_T$ , between 10 and 20  $\mu\text{mol kg}^{-1}$ , is often  
 772 recognized (Figure 11), the evaluation of the trends over more than 20 years indicated faster trend in the  
 773 subtropical Indian Ocean ( $+1.1 \mu\text{mol kg}^{-1} \text{ yr}^{-1}$ ) compared to higher latitudes (Indian POOZ,  $+0.6 \mu\text{mol kg}^{-1} \text{ yr}^{-1}$ );  
 774 they are close to the expected anthropogenic signal in these regions ( $+1.1 \mu\text{mol kg}^{-1} \text{ yr}^{-1}$  in the subtropics and  
 775  $+0.8 \mu\text{mol kg}^{-1} \text{ yr}^{-1}$  at higher latitudes).

776

777  
778  
779  
780  
781  
782  
783  
784  
785  
786  
787  
788  
789  
790  
791  
792  
793  
794  
795  
796  
797  
798

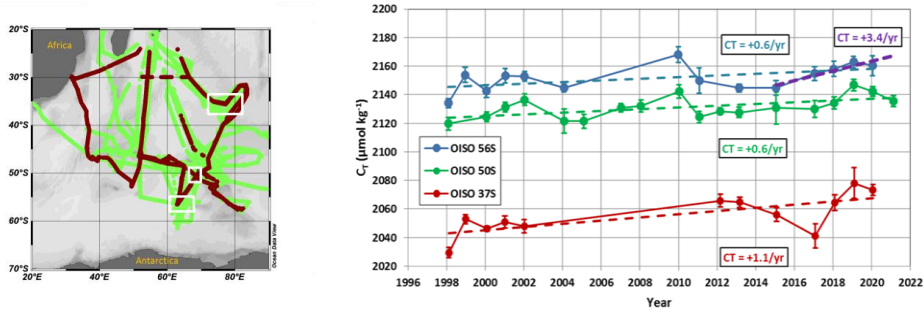


**Figure 11:** Left: Data in SNAPO-CO2-v1 dataset (green) and new data in version v2 (brown) in the South Western Indian Ocean (OISO cruises). Figure produced with ODV (Schlitzer, 2018). The white boxes identified the regions of data selected around 37°S, 50°S and 56°S for the trend analysis. Right: Time-series of average  $C_T$  concentrations in January-February at 37°S (red), 50°S (green) and 56°S (blue). The trends for each region are indicated (see also Table 7).

Mis en forme : Justifié, Espace Après : 0 pt, Interligne : simple

799 **Table 7:** Trend of  $C_T$  ( $\mu\text{mol kg}^{-1} \text{yr}^{-1}$ ) and corresponding standard error in selected regions where data are  
800 available for more than 10 years. The projects/cruises for selection of the data in each domain are indicated.

Mis en forme : Gauche, Interligne :  
Multiple 1,15 li

Mis en forme : Couleur de police :  
Rouge foncé

Region	Period/Season	$C_T$ trend ( $\mu\text{mol kg}^{-1} \text{yr}^{-1}$ )	Projects/Cruises
North Atlantic (NASPG)	1994-2023 April	+0.78 (0.23)	SURATLANT
North Atlantic (NASPG)	1994-2023 September	+1.09 (0.37)	SURATLANT
West. Trop. Atl. 5N-Eq	2009-2021 April-October	+3.31 (2.13)	AMAZOMIX, PIRATA-BR, TARA
West. Trop. Atl. Eq-10S	2005-2015 April-October	+3.05 (1.64)	CAMFIN-WAT, PIRATA-BR, VOS
Ligurian Sea 8E	1998-2022 Jan-Feb.	+0.94 (0.64)	ANTARES, DYFAMED, MOOSE-GE
Ligurian Sea 8E	1998-2023 July-August	+1.53 (0.46)	ANTARES, DYFAMED, MOOSE-GE
Subtropical Indian 37S	1998-2020 Jan-Feb.	+1.12 (0.36)	OISO
South West. Indian 50S	1998-2021 Jan-Feb.	+0.61 (0.21)	OISO
South West. Indian 56S	1998-2020 Jan-Feb.	+0.58 (0.27)	OISO
South West. Indian 56S	2015-2020 Jan-Feb.	+3.41 (0.73)	OISO
South East. Indian 60S	2002-2012 Jan-Feb.	+3.37 (0.94)	MINERVE, OISO
South East. Indian 60S	2002-2012 October	+4.79 (1.62)	MINERVE

## 826 5.5 The Coastal Zones

827  
828 Coastal waters experience enhanced ocean acidification due to increasing  $\text{CO}_2$  uptake, accumulation of  
829 anthropogenic  $\text{CO}_2$  (Bourgeois et al 2016; Laruelle et al, 2018; Roobaert et al, 2024a; Li et al, 2024) and from  
830 local anthropogenic inputs through rivers or from air pollution (e.g. Sarma et al, 2015; Sridvi and Sarma, 2021;  
831 Wimart-Rousseau et al, 2020). The changes of the  $\text{CO}_2$  uptake in coastal zones are also linked to biological  
832 processes (Mathis et al, 2024) or to circulation and local upwelling (Roobaert et al, 2024b), all controlling large  
833 variability of  $A_T$  and  $C_T$  in space and time leading to uncertainties for detecting long-term changes of  $p\text{CO}_2$  and  
834 air-sea  $\text{CO}_2$  fluxes in heterogeneous coastal waters (Dai et al 2022; Resplandy et al, 2024). At seasonal scale,  
835 large differences between observations and models were also identified leading to differences in the coastal  
836 ocean  $\text{CO}_2$  sink up to 60% (Resplandy et al, 2024). It is thus important to document the seasonal cycles of  $A_T$  and  
837  $C_T$  to compare and correct models and thus to better predict future changes of biogeochemical properties in  
838 coastal waters and their impact on marine ecosystems. A better understanding of the processes and their  
839 retroaction in the coastal regions is also required regarding Marine Carbon Dioxide Removal (MCDR)  
840 experiments and for their evaluation (e.g. Ho et al, 2023).

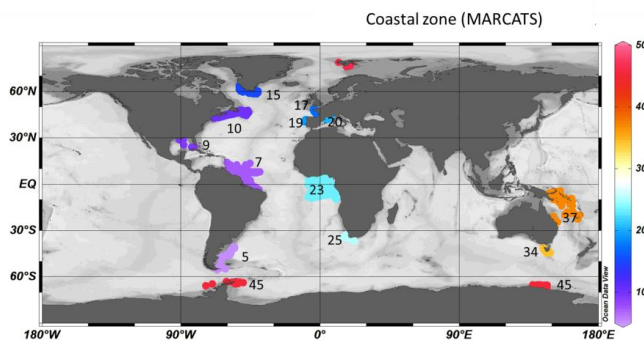
841 In the SNAPO-CO2-v2 dataset new data have been added in the coastal zones at stations SOMLIT-  
842 Brest, SOMLIT-Roscoff and SOMLIT-Point-B. They extend the period to 2022 or 2023 for temporal analysis.  
843 New data in the French coastal zones have been also included from the COCORICO2 project documented in  
844 detail by Petton et al (2024). The observations in coastal zones could be identified in the MARCATS regions  
845 (Margins and CATchment Segmentation, Laruelle et al, 2013) (Figure 12) where little information is available  
846 for quantifying the ocean  $\text{CO}_2$  sink at the decadal scale and for evaluation of the anthropogenic  $\text{CO}_2$  uptake  
847 (Regnier et al, 2013; Dai et al, 2022; Li et al, 2024). To explore the change of the observed properties in the  
848 coastal zones and have a flavor of the long-term  $C_T$  trends we selected the time series with at least 10 years of  
849 data (Table 8, Figure 13). Except at high latitudes (Greenland and Antarctic coastal zones), we observed a  
850 warming in coastal zones (not shown). Changes in salinity are also identified (increase or decrease) and results

851 of the trends are presented for salinity-normalized  $C_T$  at 34, 35 or 38 depending on the region. Although the  
 852 inter-annual variability is large in coastal waters, sometimes linked to extreme events (e.g. river discharges), we  
 853 observed an increase in  $N-C_T$  at most of the 8 selected locations. The exceptions are the coastal zones in the Gulf  
 854 of Lion near the Rhone River and near Tasmania in October.

855 In the Gulf of Lion, the new data in the coastal zone confirmed the first view at the SOLEMIO station  
 856 over 2016-2018 (Bay of Marseille, Wimart-Rousseau et al, 2020). In this region the lowest  $C_T$  was observed in  
 857 summer 2022 (average  $C_T$  of  $2238.6 \pm 21.0 \mu\text{mol kg}^{-1}$ ), much lower than in 2015 ( $2290.8 \pm 44.7 \mu\text{mol kg}^{-1}$ ). Over  
 858 the continental shelf south of Tasmania (MARCATS #34), the trend in  $N-C_T$  was positive in summer but not  
 859 significant in October. In October this was associated with an increase in Salinity and in  $A_T$  probably linked to  
 860 advective processes via the reversal and variability of the Zeehan or the East Australian currents. From our data a  
 861 warming of  $+0.06^\circ\text{C yr}^{-1}$  was identified for both seasons over 2002-2012 as previously observed south of  
 862 Tasmania over 1991-2003 impacting the  $p\text{CO}_2$  trend and air-sea  $\text{CO}_2$  fluxes in this region (Borges et al, 2008).  
 863 The difference in the  $N-C_T$  trends in austral summer and spring calls for new ~~detail~~detailed studies with extended  
 864 data in this region. At high latitude in the Adélie Land (Antarctic coast MARCATS #45), the variability of  $N-C_T$   
 865 was large (range from 2150 to 2200  $\mu\text{mol kg}^{-1}$ , Figure 13) and the trend over 10 years in summer was not  
 866 significant (Table 8). As opposed to the open zone at  $60^\circ\text{S}$  (Figure 10) the  $C_T$  concentrations in the coastal zone  
 867 near Antarctica were not increasing, probably linked to competitive processes between anthropogenic uptake,  
 868 changes in primary production, mixing or ice melting (Shadwick et al, 2013, 2014). More data are needed to  
 869 better evaluate the changes of the carbonate system in Antarctic coastal zones where bottom waters are formed  
 870 and transport anthropogenic  $\text{CO}_2$  at lower latitudes (Zhang et al, 2023).

871 For the coastal time series SOMLIT where annual trends could be estimated (sampling at monthly  
 872 resolution), the  $N-C_T$  increase ( $+2.1$  to  $3.4 \mu\text{mol kg}^{-1} \text{yr}^{-1}$ ) is close or higher than the anthropogenic signal leading  
 873 to a decrease in pH ranging between  $-0.05$  to  $-0.06$  TS decade $^{-1}$ . The new data added in the SNAPO-CO2-v2  
 874 dataset (2016-2023) confirm the progressive increase in  $C_T$  and the acidification in the western Mediterranean  
 875 Sea and in the North-East Atlantic coastal zones (Kapsenberg et al, 2017; Gac et al, 2021).

876  
877  
878  
879  
880  
881  
882  
883  
884  
885  
886  
887  
888  
889  
890  
891  
892



889 **Figure 12:** Location of  $A_T$  and  $C_T$  data available in the coastal zones in the SNAPO-CO2-v2 dataset. Numbers  
 890 and Color code identify MARCATS region (Laruelle et al, 2013). Figure produced with ODV (Schlitzer, 2018).

893  
894  
895  
896  
897  
898  
899  
900  
901  
902  
903  
904  
905  
906  
907  
908  
909  
910  
911  
912  
913  
914  
915  
916  
917  
918  
919  
920  
921  
922  
923  
924  
925  
926  
927  
928  
929  
930  
931  
932  
933  
934  
935

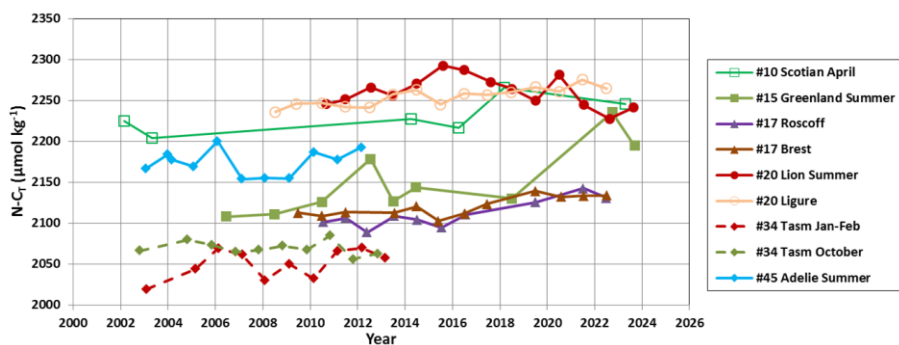


**Figure 13:** Time-series of average  $N-C_T$  concentrations ( $\mu\text{mol kg}^{-1}$ ) in selected MARCATS regions for different period when data are available for ten years or more. The trends and periods for each region are indicated in Table 8.

**Table 8:** Trends of  $N-C_T$  ( $\mu\text{mol kg}^{-1} \text{yr}^{-1}$ ) and corresponding standard errors in selected coastal regions where data are available for 10 years or more. The projects/cruises for selection of the data in each domain are indicated. MARCATS # regions also identified. Salinity value values used for  $C_T$  normalization are indicated.

Region #MARCATS	Period	Season	$N-C_T$ Trend ( $\mu\text{mol kg}^{-1} \text{yr}^{-1}$ )	Salinity	Projects/Cruises
Scotian #10	2002-2023	March-April	+1.71 (0.97)	35	SURATLANT
Greenland #15	2006-2023	June-mid-Sept	+5.77 (1.62)	35	OVIDE, SURATLANT
Roscoff #17	2010-2022	All season	+3.40 (0.76)	35	CHANNEL, COCORICO2, SOMLIT ROSCOFF
Bay of Brest #17	2009-2022	All seasons	+2.17 (0.52)	35	SOMLIT-Brest, COCORICO2, ECOSCOPA,
LION#20	2010-2023	June-Sept	-1.19 (1.25)	38	COCORICO2, MOOSE-GE, SOLEMIO (a)
LIGURE#20	2008-2022	All seasons	+2.12 (0.36)	38	SOMLIT-Point-B, MOOSE-GE
Tasmania #34	2003-2013	Jan-Feb	+2.73 (1.72)	35	MINERVE, OISO
Tasmania #34	2002-2012	Oct	-0.65 (0.89)	35	MINERVE, OISO
Adélie #45	2002-2012	Dec-Feb	+0.63 (0.70)	34	MINERVE, OISO

(a) For LION, some data in summer were also used from punctual cruises: AMOR-BFlux, CARBORHONE, DICASE, LATEX, MESURHOBENT, MISSRHODIA2 and MOLA.

Mis en forme : Gauche, Espace Après : 10 pt, Interligne : Multiple 1,15 li

## 936 6 Summary and suggestions

937

938 This work extends in time and [in](#) new oceanic regions the  $A_T$  and  $C_T$  data presented in the first SNAPO-  
939 CO<sub>2</sub> synthesis (Metzl et al, 2024a). It includes now more than 67 000 surface and water column observations in  
940 all oceanic basins, in the Mediterranean Sea, in the coastal zones, near coral reefs, and in rivers. The data  
941 synthesized in version v2 are based on measurements of  $A_T$  and  $C_T$  performed between 1993 and 2023 with an  
942 accuracy of  $\pm 4 \mu\text{mol kg}^{-1}$ . Based on a secondary quality control, 91% of the  $A_T$  and  $C_T$  data are considered as  
943 good (WOCE Flag 2) and 6% probably good (Flag 3). For the open ocean this synthesis complements the  
944 SOCAT, GLODAP and SPOTS data products (Bakker et al., 2016; Lauvset et al., 2024; Lange et al, 2024). For  
945 the coastal sites this also complements the synthesis of coastal time-series in the Iberian Peninsula (Padin et al,  
946 2020), in the Canadian Atlantic continental shelf (Gibb et al, 2023) and around North America (Fassbender et al.,  
947 2018; Jiang et al., 2021; Jiang et al 2024, in prep). The SNAPO-CO<sub>2</sub> dataset enables to investigate the seasonal  
948 cycles, the inter-annual variability and the decadal trends of  $A_T$  and  $C_T$  in various oceanic provinces. The same  
949 temporal analyses could be investigated for other carbonate system properties such as  $f\text{CO}_2$  or pH calculated  
950 from  $A_T$  and  $C_T$  for air-sea CO<sub>2</sub> flux estimates or ocean acidification studies (Figure 14).

951

952

953

954

955

956

957

958

959

960

961

962

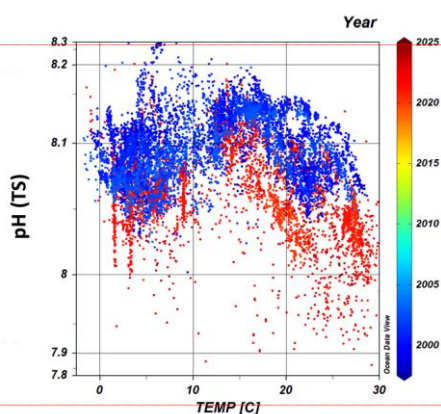
963

964

965

966

967



Mis en forme : Couleur de police : Violet

Mis en forme : Interligne : simple

Mis en forme : Couleur de police : Rouge foncé

968 **Figure 14:** An example of observed ocean acidification derived from the SNAPO-CO<sub>2</sub>-v2 dataset: pH (TS)  
969 calculated with  $A_T$  and  $C_T$  data are presented as a function of temperature (°C) for years 1998-2002 (blue  
970 symbols) and 2020-2023 (red symbols) and for salinity > 33 (Nb data selected with flag 2 = 11994). In recent  
971 years the pH was lower. Figure produced with ODV (Schlitzer, 2018).  
972

973 In almost all regions the new data in 2021-2023 indicated that the  $C_T$  concentrations were higher in  
974 recent years. In regions where data are available for more than 2 decades, the time-series show an increase of sea  
975 surface  $C_T$  (North Atlantic, Southern Indian Ocean and Ligurian Sea) with a rate close to or higher than the  
976 changes expected from anthropogenic CO<sub>2</sub> uptake. It is also recognized that at seasonal scale the  $C_T$  trends could  
977 be different. However, with the data in hand, the long-term trend of  $C_T$  cannot be quantified with confidence to  
978 compare with the anthropogenic carbon uptake in some regions. This is the case in the eastern tropical Atlantic  
979 subject to high inter-annual variability (Lefèvre et al., 2021, 2024) although new data have been added over  
980 2005-2022 in this region (Table 1, Figure S9). When data are available for less than a decade the increase in  $C_T$   
981 was observed but the trend was uncertain due to large inter-annual variability (e.g. Adélie Land). An exception  
982 was identified in the coastal zone in the Gulf of Lion (Mediterranean Sea) where summer data since 2010 present

983 a decrease in  $C_T$  most pronounced since 2015 ( $C_T$  trend =  $-5.2 \pm 1.5 \mu\text{mol kg}^{-1} \text{yr}^{-1}$ ). Such  $C_T$  decrease over 10  
984 years was also observed at the Hawaii Ocean Time series, HOT over 2010-2020 (Dore et al, 2009,  
985 <https://hahana.soest.hawaii.edu/hot/hotco2/hotco2.html>, last access: 27 August 2024).

986 Although the  $A_T$  concentrations present significant inter-annual variability such as in the NASPG, in the  
987 Topical Atlantic or the Adélie land and coastal zones,  $A_T$  appears relatively constant over time except at these  
988 locations. In the open ocean, we observed an increase of  $A_T$  in the Southern Ocean south of the Polar Front  
989 around 60°S in 2003-2012 not directly linked to salinity. In the coastal zones a decrease of  $A_T$  was pronounced  
990 south of Greenland. In the coast in the Gulf of Lion, as observed for  $C_T$ ,  $A_T$  decreased ( $A_T$  trend =  $-2.8 \pm 1.2 \mu\text{mol}$   
991  $\text{kg}^{-1} \text{yr}^{-1}$ ). This is opposed to the changes observed in the Ligurian Sea at station SOMLIT-Point-B, where  $C_T$  and  
992  $A_T$  increased over 2007-2015 (Kapsenberg et al, 2017) highlighting the contrasting  $C_T$  and  $A_T$  trends in the  
993 Mediterranean coastal zones where ocean acidification is detected (here over 2008-2022, pH trend of  $-0.048$   
994  $\pm 0.003 \text{decade}^{-1}$ ). With the continuous warming, reduced stratification and the rapid pH change observed in the  
995 Mediterranean Sea, how the marine ecosystems will respond in the future should be addressed (e.g. Howes et al,  
996 2015; Maugendre et al 2015; Lacoue-Labarthe et al, 2016). The SNAPO-CO2-v2 dataset could also be used to  
997 explore and analyze the changes of the carbonate system occurring during extreme events such as marine heat  
998 waves, rapid freshening, deep convection or high phytoplankton bloom events.

999 This dataset ~~would~~ could also serve for validating autonomous platforms capable of measuring pH and  
1000  $f\text{CO}_2$  properties (Sarmiento et al, 2023) and, along with other synthesis products (Jiang et al, 2024 in prep.),  
1001 provides an additional reference dataset for the development and validation of regional biogeochemical models  
1002 for simulating air-sea  $\text{CO}_2$  fluxes. Thanks to the RECCAP2 stories, it has been recognized that Ocean  
1003 Biogeochemical Models present biases in the seasonal cycle of  $C_T$  and  $A_T$  due to inadequate representation of  
1004 biogeochemical cycles (e.g. Hauck et al, 2023; Rodgers et al, 2023; Sarma et al, 2023; Pérez et al, 2024;  
1005 Resplandy et al, 2024). The SNAPO-CO2-v2 dataset could be used to guide analyses for regional or global  
1006 biogeochemical models for  $A_T$  and  $C_T$  comparison and validation from seasonal to decadal scales. Our dataset is  
1007 also essential for training and validating neural networks capable of predicting variables in the carbonate system  
1008 (e.g. Fourier et al, 2020; Chau et al, 2024a; Gregor et al, 2024), thereby enhancing observations of marine  $\text{CO}_2$  at  
1009 different spatial and temporal scales. Furthermore, we encourage the use of this dataset (or part of it), at sea or  
1010 prior going to sea for cruise planning. Indeed, using the approach of Davis and Goyet (2021) which takes into  
1011 account the multiple constraints (ship-time, number of samples, etc.), it is possible to determine the most  
1012 appropriate sampling strategy (Guglielmi et al., 2022, 2023), to reach the specific scientific objectives of each  
1013 cruise.

1014 The data presented here are available online on the Seano server (<https://doi.org/10.17882/102337>) in a  
1015 file identifying version v1 and v2. The sources of the original datasets (doi) with the associated references are  
1016 listed in the Supplementary Material (Tables S3, S4). As for version v1 we invite the users to comment on any  
1017 anomaly that would have not been detected or to suggest potential misqualification of data in the present product  
1018 (e.g. data probably good although assigned with flag 3, probably wrong). As for SOCAT or GLODAP, we  
1019 expect to update the SNAPO-CO2 dataset once new observations are obtained and controlled.

1020

1021 **7 Data availability**

1022 Data presented in this study are available at Seanoe (Metzl et al, 2024d, <https://www.seanoe.org>,  
1023 <https://doi.org/10.17882/102337>. See also <https://doi.org/10.17882/95414> for version V1. The dataset is also  
1024 available at <https://explore.webodv.awi.de/ocean/carbon/snapo-co2/>  
1025

1026 *Author contributions.* NM prepared the data synthesis, the figures and wrote the draft of the manuscript with  
1027 contributions from all authors. JF measured the discrete samples since 2014, with the help from CM and CLM,  
1028 and prepared the individual reports for each project. NM and JF pre-qualified the discrete  $A_T/C_T$  data. CLM and  
1029 NM are co-Is of the ongoing OISO project and qualified the underway  $A_T/C_T$  data from OISO cruises. FT and  
1030 CG were PIs of the MINERVE cruises. All authors have contributed either to organizing cruises, sample  
1031 collection and/or data qualification, and reviewed the manuscript.

1032  
1033 *Competing interest.* The authors have the following competing interests: At least one of the (co-)authors is a  
1034 member of the editorial board of Earth System Science Data  
1035

1036 *Acknowledgments.* Most of the  $A_T$  and  $C_T$  data presented in this study were measured at the SNAPO-CO2 facility  
1037 (Service National d'Analyse des Paramètres Océaniques du CO2) housed by the LOCEAN laboratory and part of  
1038 the OSU ECCE Terra at Sorbonne University and INSU/CNRS analytical services. Support by INSU/CNRS, by  
1039 OSU ECCE Terra and by LOCEAN, is gratefully acknowledged as well as support by different French "Services  
1040 nationaux d'Observations", such as OISO/CARAUS, SOMLIT, PIRATA, SSS and MOOSE. We thank the  
1041 research infrastructure ICOS (Integrated Carbon Observation System) France for funding a large part of the  
1042 analyses. We thank the IRD (Institut de Recherche pour le Développement) and the French-Brazilian IRD-  
1043 FAPEMA program for funding observations in the tropical Atlantic. We thank the French oceanographic fleet  
1044 ("Flotte océanographique française") for financial and logistic support for most cruises listed in this synthesis  
1045 and for the OISO program (<https://campagnes.flotteoceanographique.fr/series/228/>). We acknowledge the  
1046 MOOSE program (Mediterranean Ocean Observing System for the Environment, <https://campagnes.flotteoceanographique.fr/series/235/fr/>) coordinated by CNRS-INSU and the Research  
1047 Infrastructure ILICO (CNRS-IFREMER). The CocoriCO2 project was founded by European Maritime and  
1048 Fisheries Fund (grant no. 344, 2020–2023) and benefited from a subsidy from the Adour-Garonne water agency.  
1049 We thank the following programs coordinated by A. Tribollet which have contributed to the acquisition of the  
1050 data in Mayotte: CARBODISS funded by CNRS-INSU in 2018-2019, Future Maore reefs funded by Next  
1051 Generation UE-France Relance in 2021-2023, and OA-ME funded by a Belmont Forum International (ANR) in  
1052 2020-2026. We thank the program Mermex-Mistrals CNRS for supporting AMOR-BFlux, CARBORHONE,  
1053 DICASE and MESURHOBENT cruises and the program EC2CO-INSU for supporting MISSRHODIA2 cruise.  
1054 The ACCESS project was supported by CNRS MISTRALS and the DELTARHONE-1 by EC2CO-INSU. The  
1055 ACIDHYPO project was founded by CNRS International Emerging Actions; we thank Captain and crew of the  
1056 R/V Savannah from the Skidaway Institute of Oceanography (University of Georgia) for their support and  
1057 technical assistance during the operations at sea. The AMAZOMIX project was funded by French  
1058 Oceanographic Fleet, INSU (LEFE), IRD (LMI TAPICOA), CNES (TOSCA MIAMAZ project) and by the  
1059 French-Brazilian international program GUYAMAZON. The OISO program was supported by the French  
1060 institutes INSU (Institut National des Sciences de l'Univers) and IPEV (Institut Polaire Paul-Emile Victor), OSU  
1061



1062 Ecce-Terra (at Sorbonne Université), and the French program SOERE/Great-Gases. We also thank the Research  
1063 Infrastructure ILICO (<https://www.ir-ilico.fr>). We warmly thank Alain Poisson who initiated the MINERVE  
1064 program and performed many of the measurements onboard R/V Astrolabe from 2002 through 2018. We thank  
1065 all colleagues and students who participated to the cruises and have carefully collected the precious seawater  
1066 samples. We thank Frédéric Merceur (IFREMER) for preparing the page and data availability on Seanoe and  
1067 Reiner Schlitzer (AWI) for including the SNAPO-CO2 dataset in the ODV portal. [We thank the associated editor  
1068 Sebastiaan van de Velde to manage this manuscript, and Kim Currie and Toste Tanhua for their suggestions that  
1069 helped to improve this article.](#)

1070  
1071

## 1072 **References:**

1073

1074 Ait Ballagh, F.E., Rabouille, C., Andrieux-Loyer, F. et al. Spatial Variability of Organic Matter and Phosphorus  
1075 Cycling in Rhône River Prodelta Sediments (NW Mediterranean Sea, France): a Model-Data Approach.  
1076 *Estuaries and Coasts* 44, 1765–1789, <https://doi.org/10.1007/s12237-020-00889-9>, 2021

1077

1078 Álvarez, M., Catalá, T. S., Civitarese, G., Coppola, L., Hassoun, A. E.R., Ibello, V., Lazzari, P., Lefevre, D.,  
1079 Macías, D., Santinelli, C. and Ulses, C.: Chapter 11 - Mediterranean Sea general biogeochemistry, Editor(s):  
1080 Katrin Schroeder, Jacopo Chiggiato, *Oceanography of the Mediterranean Sea*, Elsevier, Pages 387-451,  
1081 <https://doi.org/10.1016/B978-0-12-823692-5.00004-2>, 2023.

1082

1083 Bakker, D. C. E., Pfeil, B., Landa, C. S., Metzl, N., O'Brien, K. M., Olsen, A., Smith, K., Cosca, C., Harasawa,  
1084 S., Jones, S. D., Nakaoka, S.-I., Nojiri, Y., Schuster, U., Steinhoff, T., Sweeney, C., Takahashi, T., Tilbrook, B.,  
1085 Wada, C., Wanninkhof, R., Alin, S. R., Balestrini, C. F., Barbero, L., Bates, N. R., Bianchi, A. A., Bonou, F.,  
1086 Boutin, J., Bozec, Y., Burger, E. F., Cai, W.-J., Castle, R. D., Chen, L., Chierici, M., Currie, K., Evans, W.,  
1087 Featherstone, C., Feely, R. A., Fransson, A., Goyet, C., Greenwood, N., Gregor, L., Hankin, S., Hardman-  
1088 Mountford, N. J., Harlay, J., Hauck, J., Hoppema, M., Humphreys, M. P., Hunt, C. W., Huss, B., Ibáñez, J. S.  
1089 P., Johannessen, T., Keeling, R., Kitidis, V., Körtzinger, A., Kozyr, A., Krasakopoulou, E., Kuwata, A.,  
1090 Landschützer, P., Lauvset, S. K., Lefèvre, N., Lo Monaco, C., Manke, A., Mathis, J. T., Merlivat, L., Millero, F.  
1091 J., Monteiro, P. M. S., Munro, D. R., Murata, A., Newberger, T., Omar, A. M., Ono, T., Paterson, K., Pearce, D.,  
1092 Pierrot, D., Robbins, L. L., Saito, S., Salisbury, J., Schlitzer, R., Schneider, B., Schweitzer, R., Sieger, R.,  
1093 Skjelvan, I., Sullivan, K. F., Sutherland, S. C., Sutton, A. J., Tadokoro, K., Telszewski, M., Tuma, M., Van  
1094 Heuven, S. M. A. C., Vandemark, D., Ward, B., Watson, A. J., and Xu, S.: A multi-decade record of high-quality  
1095 fCO<sub>2</sub> data in version 3 of the Surface Ocean CO<sub>2</sub> Atlas (SOCAT), *Earth Syst. Sci. Data*, 8, 383-413,  
1096 doi:10.5194/essd-8-383-2016. 2016.

1097

1098 Barral, Q-B., Zakardjian, B. Dumas, F., Garreau, P., Testor, P., and Beuvier, J.: Characterization of fronts in the  
1099 Western Mediterranean with a special focus on the North Balearic Front, *Progress in Oceanography*, Volume  
1100 197, 102636, <https://doi.org/10.1016/j.pocean.2021.102636>. 2021

1101

1102 Barré, L., Diaz, F., Wagener, T., Van Wambeke, F., Mazoyer, C., Yohia, C., and Pinazo, C.: Implementation and  
1103 assessment of a model including mixotrophs and the carbonate cycle (Eco3M\_MIX-CarbOx v1.0) in a highly  
1104 dynamic Mediterranean coastal environment (Bay of Marseille, France) – Part 1: Evolution of ecosystem  
1105 composition under limited light and nutrient conditions, *Geosci. Model Dev.*, 16, 6701–6739,  
1106 <https://doi.org/10.5194/gmd-16-6701-2023>, 2023.

1107

1108 Barré, L., Diaz, F., Wagener, T., Mazoyer, C., Yohia, C., and Pinazo, C.: Implementation and assessment of a  
1109 model including mixotrophs and the carbonate cycle (Eco3M\_MIX-CarbOx v1.0) in a highly dynamic  
1110 Mediterranean coastal environment (Bay of Marseille, France) – Part 2: Towards a better representation of total  
1111 alkalinity when modeling the carbonate system and air–sea CO<sub>2</sub> fluxes, *Geosci. Model Dev.*, 17, 5851–5882,  
1112 <https://doi.org/10.5194/gmd-17-5851-2024>, 2024.

1113

1114 BERTRAND Arnaud, DE SAINT LEGER Emmanuel, KOCH-LARROUY Ariane : AMAZOMIX 2021 cruise,  
1115 RV Antea, <https://doi.org/10.17600/18001364>, 2021  
1116  
1117 Bittig, H.C., Steinhoff, T., Claustre, H., Fiedler, B., Williams, N.L., Sauzède, R., Körtzinger, A. and Gattuso, J.-  
1118 P.: An Alternative to Static Climatologies: Robust Estimation of Open Ocean CO<sub>2</sub> Variables and Nutrient  
1119 Concentrations From T, S, and O<sub>2</sub> Data Using Bayesian Neural Networks. *Front. Mar. Sci.* 5:328. doi:  
1120 10.3389/fmars.2018.00328, 2018  
1121  
1122 Bonou, F.K., Noriega, C., Lefèvre, N., Araujo, M.: Distribution of CO<sub>2</sub> parameters in the Western Tropical  
1123 Atlantic Ocean, *Dynamics of Atmospheres and Oceans*, 73: 47-60  
1124 <http://dx.doi.org/10.1016/j.dynatmoce.2015.12.001>, 2016  
1125  
1126 Bonou, F., Medeiros, C., Noriega, C., Araujo, M., Aubains Hounsou-Gbo, A., and Lefèvre N. : A comparative  
1127 study of total alkalinity and total inorganic carbon near tropical Atlantic coastal regions. *J Coast Conserv* 26, 31,  
1128 <https://doi.org/10.1007/s11852-022-00872-5>, 2022  
1129  
1130 Borges A.V., B. Tilbrook, N. Metzl, A. Lenton and B. Delille: Inter-annual variability of the carbon dioxide  
1131 oceanic sink south of Tasmania, *Biogeosciences*, 5, 141-155. <https://doi.org/10.5194/bg-5-141-2008>, 2008  
1132  
1133 Bourgeois, T., J. C. Orr, L. Resplandy, J. Terhaar, C. Ethé, M. Gehlen, and L. Bopp: Coastal-ocean uptake of  
1134 anthropogenic carbon. *Biogeosciences*, 13, 4167-4185, doi: 10.5194/bg-13-4167-2016., 2016  
1135  
1136 BOURLES Bernard (1997) PIRATA, <https://doi.org/10.18142/14>  
1137  
1138 BOURLES Bernard (2019) PIRATA FR29 cruise, RV Thalassa, <https://doi.org/10.17600/18000875>  
1139  
1140 BOURLES Bernard, LLIDO Jérôme (2020) PIRATA FR30 cruise, RV Thalassa,  
1141 <https://doi.org/10.17600/18000690>  
1142  
1143 BOURLES Bernard, LLIDO Jérôme (2022) PIRATA FR32 cruise, RV Thalassa,  
1144 <https://doi.org/10.17600/18001832>  
1145  
1146 Bozec Y., Cariou, T., Mace, E., Morin, P., Thuillier, D., Vernet, M.: Seasonal dynamics of air-sea CO<sub>2</sub> fluxes in  
1147 the inner and outer Loire estuary (NW Europe). *Estuarine Coastal And Shelf Science*, 100, 58-71.  
1148 <https://doi.org/10.1016/j.ecss.2011.05.015>, 2012  
1149  
1150 BOZEC Yann (2009) CO<sub>2</sub>ARVOR 3 cruise, RV Côtes De La Manche, <https://doi.org/10.17600/9480170>  
1151  
1152 BOZEC Yann (2009) CO<sub>2</sub>ARVOR 2 cruise, RV Côtes De La Manche, <https://doi.org/10.17600/9480110>  
1153  
1154 BOZEC Yann (2009) CO<sub>2</sub>ARVOR 1 cruise, RV Thalia, <https://doi.org/10.17600/9070070>  
1155  
1156 Brandon, M., C. Goyet, F. Touratier, N. Lefèvre, E. Kestenare, and R. Morrow : Spatial and temporal variability  
1157 of the physical, carbonate and CO<sub>2</sub> properties in the Southern Ocean surface waters during austral summer  
1158 (2005-2019). *Deep Sea Res. Part I*, 187, 103836, <https://doi.org/10.1016/j.dsr.2022.103836>. 2022  
1159  
1160 Broullón, D., Pérez, F. F., Velo, A., Hoppema, M., Olsen, A., Takahashi, T., Key, R. M., Tanhua, T., González-  
1161 Dávila, M., Jeansson, E., Kozyr, A., and van Heuven, S. M. A. C.: A global monthly climatology of total  
1162 alkalinity: a neural network approach, *Earth Syst. Sci. Data*, 11, 1109–1127, [https://doi.org/10.5194/essd-11-](https://doi.org/10.5194/essd-11-1109-2019)  
1163 1109-2019. 2019  
1164

1165 Broullón, D., Pérez, F. F., Velo, A., Hoppema, M., Olsen, A., Takahashi, T., Key, R. M., Tanhua, T., Santana-  
1166 Casiano, J. M., and Kozyr, A.: A global monthly climatology of oceanic total dissolved inorganic carbon: a  
1167 neural network approach, *Earth Syst. Sci. Data*, 12, 1725–1743, <https://doi.org/10.5194/essd-12-1725-2020>.  
1168 2020  
1169  
1170 CARIOU Thierry, BOZEC Yann (2010) CO2ARVOR 4 cruise, RV Thalia, <https://doi.org/10.17600/10070040>  
1171  
1172 Carter, B. R., Feely, R. A., Williams, N. L., Dickson, A. G., Fong, M. B., and Takeshita, Y.: Updated methods  
1173 for global locally interpolated estimation of alkalinity, pH, and nitrate. *Limnology and Oceanography: Methods*,  
1174 16: 119-131. doi: 10.1002/lom3.10232, 2018  
1175  
1176 Chau, T.-T.-T., Gehlen, M., Metzl, N., and Chevallier, F.: CMEMS-LSCE: a global, 0.25°, monthly  
1177 reconstruction of the surface ocean carbonate system, *Earth Syst. Sci. Data*, 16, 121–160,  
1178 <https://doi.org/10.5194/essd-16-121-2024>, 2024a.  
1179  
1180 Chau, T.-T.-T., Chevallier, F., and Gehlen, M.: Global analysis of surface ocean CO2 fugacity and air-sea fluxes  
1181 with low latency. *Geophysical Research Letters*, 51, e2023GL106670. <https://doi.org/10.1029/2023GL106670>,  
1182 2024b  
1183  
1184 Cheng, L. J., Abraham, J., Zhu, J., Trenberth, K. E., Fasullo, J., Boyer, T., Locarnini, R., Zhang, B., Yu, F. J.,  
1185 Wan, L. Y., Chen, X. R., Song, X. Z., Liu, Y. L., and Mann, M. E.: Record-setting ocean warmth continued in  
1186 2019, *Adv. Atmos. Sci.*, 37, 137-142. <https://doi.org/10.1007/s00376-020-9283-7>, 2020  
1187  
1188 Cheng, L., Abraham, J., Trenberth, K.E. et al. New Record Ocean Temperatures and Related Climate Indicators  
1189 in 2023. *Adv. Atmos. Sci.*, <https://doi.org/10.1007/s00376-024-3378-5>, 2024  
1190  
1191 Conan, P., Guieux, A., and Vuillemin, R.: MOOSE (MOLA), <https://doi.org/10.18142/234>, 2020.  
1192  
1193 Copin-Montégut, C.: Alkalinity and carbon budgets in the Mediterranean Sea, *Global Biogeochemical Cycles*,  
1194 vol. 7, pp. 915–925, 1993.  
1195  
1196 Coppola, L., and Diamond-Riquier, E.: MOOSE (DYFAMED), <https://doi.org/10.18142/131>, 2008.  
1197  
1198 Coppola Laurent, Diamond Riquier Emilie, Carval Thierry, Irisson Jean-Olivier, Desnos Corinne: Dyfamed  
1199 observatory data. SEANO. <https://doi.org/10.17882/43749>, 2024  
1200  
1201 Coppola, L., Fourier, M., Pasqueron de Fommervault, O., Poteau, A., Riquier, E. D. and Béguery, L.:  
1202 Highresolution study of the air-sea CO2 flux and net community oxygen production in the Ligurian Sea by a  
1203 fleet of gliders. *Front. Mar. Sci.* 10:1233845. doi: 10.3389/fmars.2023.1233845, 2023  
1204  
1205 Curbelo-Hernández, D., Pérez, F. F., González-Dávila, M., Gladyshev, S. V., González, A. G., González-  
1206 Santana, D., Velo, A., Sokov, A., and Santana-Casiano, J. M.: Ocean Acidification trends and Carbonate System  
1207 dynamics in the North Atlantic Subpolar Gyre during 2009–2019, *EGUsphere* [preprint],  
1208 <https://doi.org/10.5194/egusphere-2024-1388>, 2024.  
1209  
1210 Currie, K. I., Reid, M. R., and Hunter, K. A.: Interannual variability of carbon dioxide draw-down by  
1211 subantarctic surface water near New Zealand, *Biogeochemistry*, 104, 23–34, [https://doi.org/10.1007/s10533-009-](https://doi.org/10.1007/s10533-009-9355-3)  
1212 9355-3, 2011.  
1213  
1214 Cyronak, T., Santos, I. R., Erler, D. V., and Eyre, B. D.: Groundwater and porewater as major sources of  
1215 alkalinity to a fringing coral reef lagoon (Muri Lagoon, Cook Islands), *Biogeosciences*, 10, 2467–2480,  
1216 <https://doi.org/10.5194/bg-10-2467-2013>, 2013.  
1217

1218 Dai, M., J. Su, Y. Zhao, E. E. Hofmann, Z. Cao, W. -J. Cai, J. Gan, F. Lacroix, G. G. Laruelle, F. Meng, J. D.  
1219 Müller, P. A.G. Regnier, G. Wang, Z. Wang, 2022. Carbon Fluxes in the Coastal Ocean: Synthesis, Boundary  
1220 Processes and Future Trends, *Annual Review of Earth and Planetary Sciences*, 50:1, 593-626,  
1221 <https://doi.org/10.1146/annurev-earth-032320-090746>, 2022  
1222  
1223 Davis D. and Goyet, C.: *Balanced Error Sampling with applications to ocean biogeochemical sampling.*  
1224 *Collection études, Presses Universitaires de Perpignan*, 224p. ISBN : 978-2-35412-452-6, 2021  
1225  
1226 Dickson, A. G., Sabine, C. L., and Christian, J. R.: *Guide to best practices for ocean CO<sub>2</sub> measurements*, North  
1227 Pacific Marine Science Organization, Sidney, British Columbia, 191, <https://doi.org/10.25607/OBP-1342>, 2007.  
1228  
1229 DOE: *Handbook of Methods for Analysis of the Various Parameters of the Carbon Dioxide System in Seawater;*  
1230 *version 2*, A.G. Dickson et C. Goyet, eds, ORNL/CDIAC-74, <https://doi.org/10.2172/10107773>, 1994.  
1231  
1232 Doney, S. C., Fabry, V. J., Feely, R. A., and Kleypas, J. A., Ocean acidification: The other CO<sub>2</sub> problem. *Annual*  
1233 *Review of Marine Science*, 1(1), 169–192. 10.1146/annurev.marine.010908.163834, 2009  
1234  
1235 Doney, S. C., Busch, D. S., Cooley, S. R., and Kroeker, K. J.: The Impacts of Ocean Acidification on Marine  
1236 Ecosystems and Reliant Human Communities. *Annual Review of Environment and Resources* 45:1,  
1237 <https://doi.org/10.1146/annurev-environ-012320-083019>. 2020  
1238  
1239 Dumoulin J-P, Pozzato L., Rassman J., Toussaint F., Fontugne M., Tisnerat-Laborde N., Beck L., Caffy I.,  
1240 Delque-Kolic E., Moreau C., Rabouille C. : Isotopic Signature (13C, 14C) of DIC in Sediment Pore Waters: An  
1241 Example from the Rhone River Delta. *Radiocarbon*, 60(5), 1465-1481. <https://doi.org/10.1017/RDC.2018.111>,  
1242 2018.  
1243  
1244 Dumoulin J-P, Rabouille C, Pourtout S, Bombléd B, Lansard B, Caffy I, Hain S, Perron M, Sieudat M, Thellier  
1245 B, Delqué-Kolic E, Moreau C, Beck L (2022) : Identification in Pore Waters of Recycled Sediment Organic  
1246 Matter Using the Dual Isotopic Composition of Carbon (13C and 14C): New Data From the Continental Shelf  
1247 Influenced by the Rhône River. *Radiocarbon*, 64(6), 1617-1627. <https://doi.org/10.1017/RDC.2022.71>, 2022.  
1248  
1249 Edmond, J. M.: High precision determination of titration alkalinity and total carbon dioxide content of sea water  
1250 by potentiometric titration, *Deep-Sea Res.*, 17, 737–750, [https://doi.org/10.1016/0011-7471\(70\)90038-0](https://doi.org/10.1016/0011-7471(70)90038-0), 1970.  
1251  
1252 Eyring, V., Righi, M., Lauer, A., Evaldsson, M., Wenzel, S., Jones, C., Anav, A., Andrews, O., Cionni, I., Davin,  
1253 E. L., Deser, C., Ehbrecht, C., Friedlingstein, P., Gleckler, P., Gottschaldt, K.-D., Hagemann, S., Jukes, M.,  
1254 Kindermann, S., Krasting, J., Kunert, D., Levine, R., Loew, A., Mäkelä, J., Martin, G., Mason, E., Phillips, A. S.,  
1255 Read, S., Rio, C., Roehrig, R., Senfleben, D., Sterl, A., van Ulft, L. H., Walton, J., Wang, S., and Williams, K.  
1256 D.: ESMValTool (v1.0) – a community diagnostic and performance metrics tool for routine evaluation of Earth  
1257 system models in CMIP, *Geosci. Model Dev.*, 9, 1747-1802, doi:10.5194/gmd-9-1747-2016, 2016.  
1258  
1259 Fabry, V. J., Seibel, B. A., Feely, R. A. and Orr, J. C.: Impacts of ocean acidification on marine fauna and  
1260 ecosystem processes. *ICES J. Mar. Sci.* 65, 414–432. <https://doi.org/10.1093/icesjms/fsn048>, 2008.  
1261  
1262 Faranda, D., Pascale, S., Bulut, B.: Persistent anticyclonic conditions and climate change exacerbated the  
1263 exceptional 2022 European-Mediterranean drought. *Environ. Res. Lett.*, 18, 034030, DOI 10.1088/1748-  
1264 9326/acbc37, 2023  
1265  
1266 Fassbender, A. J., Alin, S. R., Feely, R. A., Sutton, A. J., Newton, J. A., Krembs, C., Bos, J., Keyzers, M., Devol,  
1267 A., Ruef, W., and Pelletier, G.: Seasonal carbonate chemistry variability in marine surface waters of the US  
1268 Pacific Northwest, *Earth Syst. Sci. Data*, 10, 1367–1401, <https://doi.org/10.5194/essd-10-1367-2018>, 2018.  
1269

1270 Fay, A. R., and McKinley, G. A.: Global open-ocean biomes: Mean and temporal variability. *Earth System*  
1271 *Science Data*, 6(2), 273–284. <https://doi.org/10.5194/essd-6-273-2014>, 2014

1272

1273 Fourier, M., Coppola, L., Claustre, H., D’Ortenzio, F., Sauzède, R. and Gattuso, J.-P.: A regional neural  
1274 network approach to estimate water-column nutrient concentrations and carbonate system variables in the  
1275 Mediterranean Sea: CANYON-MED. *Frontiers in Marine Science*, 7:620,  
1276 <https://www.frontiersin.org/articles/10.3389/fmars.2020.00620>, 2020.

1277

1278 Friedlingstein, P., O’Sullivan, M., Jones, M. W., Andrew, R. M., Gregor, L., Hauck, J., Le Quéré, C., Luijkx, I.  
1279 T., Olsen, A., Peters, G. P., Peters, W., Pongratz, J., Schwingshackl, C., Sitch, S., Canadell, J. G., Ciais, P.,  
1280 Jackson, R. B., Alin, S. R., Alkama, R., Arneeth, A., Arora, V. K., Bates, N. R., Becker, M., Bellouin, N., Bittig,  
1281 H. C., Bopp, L., Chevallier, F., Chini, L. P., Cronin, M., Evans, W., Falk, S., Feely, R. A., Gasser, T., Gehlen,  
1282 M., Gkritzalis, T., Gloege, L., Grassi, G., Gruber, N., Gürses, Ö., Harris, I., Hefner, M., Houghton, R. A., Hurtt,  
1283 G. C., Iida, Y., Ilyina, T., Jain, A. K., Jersild, A., Kadono, K., Kato, E., Kennedy, D., Klein Goldewijk, K.,  
1284 Knauer, J., Korsbakken, J. I., Landschützer, P., Lefèvre, N., Lindsay, K., Liu, J., Liu, Z., Marland, G., Mayot, N.,  
1285 McGrath, M. J., Metzl, N., Monacci, N. M., Munro, D. R., Nakaoka, S.-I., Niwa, Y., O’Brien, K., Ono, T.,  
1286 Palmer, P. I., Pan, N., Pierrot, D., Pocock, K., Poulter, B., Resplandy, L., Robertson, E., Rödenbeck, C.,  
1287 Rodriguez, C., Rosan, T. M., Schwinger, J., Séférian, R., Shutler, J. D., Skjelvan, I., Steinhoff, T., Sun, Q.,  
1288 Sutton, A. J., Sweeney, C., Takao, S., Tanhua, T., Tans, P. P., Tian, X., Tian, H., Tilbrook, B., Tsujino, H.,  
1289 Tubiello, F., van der Werf, G. R., Walker, A. P., Wanninkhof, R., Whitehead, C., Willstrand Wranne, A.,  
1290 Wright, R., Yuan, W., Yue, C., Yue, X., Zaehle, S., Zeng, J., and Zheng, B.: Global Carbon Budget 2022, *Earth*  
1291 *Syst. Sci. Data*, 14, 4811–4900, <https://doi.org/10.5194/essd-14-4811-2022>, 2022.

1292

1293 Friedlingstein, P., O’Sullivan, M., Jones, M. W., Andrew, R. M., Bakker, D. C. E., Hauck, J., Landschützer, P.,  
1294 Le Quéré, C., Luijkx, I. T., Peters, G. P., Peters, W., Pongratz, J., Schwingshackl, C., Sitch, S., Canadell, J. G.,  
1295 Ciais, P., Jackson, R. B., Alin, S. R., Anthoni, P., Barbero, L., Bates, N. R., Becker, M., Bellouin, N., Decharme,  
1296 B., Bopp, L., Brasika, I. B. M., Cadule, P., Chamberlain, M. A., Chandra, N., Chau, T.-T.-T., Chevallier, F.,  
1297 Chini, L. P., Cronin, M., Dou, X., Enyo, K., Evans, W., Falk, S., Feely, R. A., Feng, L., Ford, D. J., Gasser, T.,  
1298 Ghattas, J., Gkritzalis, T., Grassi, G., Gregor, L., Gruber, N., Gürses, Ö., Harris, I., Hefner, M., Heinke, J.,  
1299 Houghton, R. A., Hurtt, G. C., Iida, Y., Ilyina, T., Jacobson, A. R., Jain, A., Jarníková, T., Jersild, A., Jiang, F.,  
1300 Jin, Z., Joos, F., Kato, E., Keeling, R. F., Kennedy, D., Klein Goldewijk, K., Knauer, J., Korsbakken, J. I.,  
1301 Körtzinger, A., Lan, X., Lefèvre, N., Li, H., Liu, J., Liu, Z., Ma, L., Marland, G., Mayot, N., McGuire, P. C.,  
1302 McKinley, G. A., Meyer, G., Morgan, E. J., Munro, D. R., Nakaoka, S.-I., Niwa, Y., O’Brien, K. M., Olsen, A.,  
1303 Omar, A. M., Ono, T., Paulsen, M., Pierrot, D., Pocock, K., Poulter, B., Powis, C. M., Rehder, G., Resplandy, L.,  
1304 Robertson, E., Rödenbeck, C., Rosan, T. M., Schwinger, J., Séférian, R., Smallman, T. L., Smith, S. M.,  
1305 Sospedra-Alfonso, R., Sun, Q., Sutton, A. J., Sweeney, C., Takao, S., Tans, P. P., Tian, H., Tilbrook, B., Tsujino,  
1306 H., Tubiello, F., van der Werf, G. R., van Ooijen, E., Wanninkhof, R., Watanabe, M., Wimart-Rousseau, C.,  
1307 Yang, D., Yang, X., Yuan, W., Yue, X., Zaehle, S., Zeng, J., and Zheng, B.: Global Carbon Budget 2023, *Earth*  
1308 *Syst. Sci. Data*, 15, 5301–5369, <https://doi.org/10.5194/essd-15-5301-2023>, 2023.

1309

1310 Fröb, F., Olsen, A., Becker, M., Chafik, L., Johannessen, T., Reverdin, G., and Omar, A.: Wintertime fCO<sub>2</sub>  
1311 variability in the subpolar North Atlantic since 2004. *Geophysical Research Letters*, 46,  
1312 <https://doi.org/10.1029/2018GL080554>, 2019.

1313

1314 Gac, J.-P., Marrec, P., Cariou, T., Grosstefan, E., Macé, E., Rimmelin-Maury, P., Vernet, M., and Bozec, Y.:  
1315 Decadal Dynamics of the CO<sub>2</sub> System and Associated Ocean Acidification in Coastal Ecosystems of the North  
1316 East Atlantic Ocean. *Front. Mar. Sci.* 8:688008. doi:10.3389/fmars.2021.688008, 2021.

1317

1318 Gallego, M. A., Timmermann, A., Friedrich, T., and Zeebe, R. E.: Drivers of future seasonal cycle changes in  
1319 oceanic pCO<sub>2</sub>, *Biogeosciences*, 15, 5315–5327, <https://doi.org/10.5194/bg-15-5315-2018>, 2018.

1320

1321 Gattuso, J.-P., Magnan, A., Billé, R., Cheung, W. W. L., Howes, E. L., Joos, F., Allemand, D., Bopp, L., Cooley,  
1322 S., Eakin, M., Hoegh-Guldberg, O., Kelly, R. P., Pörtner, H.-O., Rogers, A. D., Baxter, J. M., Laffoley, D.,

1323 Osborn, D., Rankovic, A., Rochette, J., Sumaila, U. R., Treyer, S., and Turley, C.: Contrasting futures for ocean  
1324 and society from different anthropogenic CO<sub>2</sub> emissions scenarios. *Science* 349:aac4722.doi:  
1325 10.1126/science.aac4722, 2015.

1326

1327 Gattuso, Jean-Pierre; Alliouane, Samir; Mousseau, Laure (2021): Seawater carbonate chemistry in the Bay of  
1328 Villefranche, Point B (France), January 2007 - June 2023 [dataset]. PANGAEA,  
1329 <https://doi.org/10.1594/PANGAEA.727120>

1330

1331 Gibb, O., Cyr, F., Azetsu-Scott, K., Chassé, J., Childs, D., Gabriel, C.-E., Galbraith, P. S., Maillet, G., Pepin, P.,  
1332 Punshon, S., and Starr, M.: Spatiotemporal variability in pH and carbonate parameters on the Canadian Atlantic  
1333 continental shelf between 2014 and 2022, *Earth Syst. Sci. Data*, 15, 4127–4162, [https://doi.org/10.5194/essd-15-](https://doi.org/10.5194/essd-15-4127-2023)  
1334 [4127-2023](https://doi.org/10.5194/essd-15-4127-2023), 2023.

1335

1336 Goyet, C., Beauverger, C., Brunet, C., and Poisson, A.: Distribution of carbon dioxide partial pressure in surface  
1337 waters of the Southwest Indian Ocean, *Tellus B: Chemical and Physical Meteorology*, 43:1, 1-11, DOI:  
1338 [10.3402/tellusb.v43i1.15242](https://doi.org/10.3402/tellusb.v43i1.15242), 1991.

1339

1340 Goyet C., Hassoun, A. E. R. Gemayel, E. Touratier, F., Abboud-Abi Saab M. and Guglielmi, V.:  
1341 Thermodynamic forecasts of the Mediterranean Sea Acidification. *Mediterranean Marine Science*, 17/2, 508-  
1342 518, <http://dx.doi.org/10.12681/mms.1487>, 2016

1343

1344 Goyet C., Benallal, M.A., Bijoux A., Guglielmi, V., Moussa, H., Ribou, A.-C., and Touratier, F.: Ch.39,  
1345 Evolution of human Impact on Oceans: Tipping points of socio-ecological Coviability. In: *Coviability of Social*  
1346 *and Ecological Systems: Reconnecting Mankind to the Biosphere in an Era of Global Change*. O.Barrière et al.  
1347 (eds.) Springer International Publishing AG, part of Springer Nature 2019. [https://doi.org/10.1007/978-3-319-](https://doi.org/10.1007/978-3-319-78111-2_12)  
1348 [78111-2\\_12](https://doi.org/10.1007/978-3-319-78111-2_12), 2019

1349

1350 Gregor, L. and Gruber, N.: OceanSODA-ETHZ: a global gridded data set of the surface ocean carbonate system  
1351 for seasonal to decadal studies of ocean acidification, *Earth Syst. Sci. Data*, 13, 777–808,  
1352 <https://doi.org/10.5194/essd-13-777-2021>, 2021.

1353

1354 Gregor, L., Shutler, J., and Gruber, N.: High-resolution variability of the ocean carbon sink. *Global*  
1355 *Biogeochemical Cycles*, 38, e2024GB008127. <https://doi.org/10.1029/2024GB008127>, 2024

1356

1357 Gruber, N., Clement, D. , Carter, B. R., Feely, R. A., van Heuven, S., Hoppema, M., Ishii, M., Key, R. M.,  
1358 Kozyr, A., Lauvset, S. K., Lo Monaco, C. , Mathis, J. T., Murata, A., Olsen, A., Perez, F. F., Sabine, C. L.,  
1359 Tanhua, T., and Wanninkhof, R.: The oceanic sink for anthropogenic CO<sub>2</sub> from 1994 to 2007, *Science* vol. 363  
1360 (issue 6432), pp. 1193-1199. DOI: 10.1126/science.aau5153, 2019.

1361

1362 Guglielmi V., Touratier, F., and Goyet, C.: Design of sampling strategy measurements of CO<sub>2</sub>/carbonate  
1363 properties. *Journal of Oceanography and Aquaculture*, DOI: 10.23880/joac-16000227, 2022

1364

1365 Guglielmi V., Touratier, F., and Goyet, C.: Determination of discrete sampling locations minimizing both the  
1366 number of samples and the maximum interpolation error: Application to measurements of carbonate chemistry in  
1367 surface ocean, *Journal of Sea Research*, <https://doi.org/10.1016/j.seares.2023.102336>, 2023

1368

1369 Hauck, J., Gregor, L., Nissen, C., Patara, L., Hague, M., Mongwe, P., et al.: The Southern Ocean carbon cycle  
1370 1985–2018: Mean, seasonal cycle, trends, and storage. *Global Biogeochemical Cycles*, 37, e2023GB007848.  
1371 <https://doi.org/10.1029/2023GB007848>, 2023

1372

1373 Ho, D. T., Bopp, L., Palter, J. B., Long, M. C., Boyd, P.W., Neukermans, G., and Bach, L. T. : Monitoring,  
1374 reporting, and verification for ocean alkalinity enhancement. *State of the Planet*, 2-oae2023, 1–12, 2023.

1375

1376 Holliday, N.P., Bersch, M., Berx, B., Chafik, L., Cunningham, S., Florindo-López, C., Hátún, H., Johns, W.,  
1377 Josey, S.A., Larsen, K.M.H., Mulet, S., Oltmanns, M., Reverdin, G., Rossby, T., Thierry, V., Valdimarsson, H.,  
1378 Yashayaev, I. : Ocean circulation causes the largest freshening event for 120 years in eastern subpolar North  
1379 Atlantic. *Nat. Commun.*, 11. <https://doi.org/10.1038/s41467-020-14474-y>, 2020  
1380  
1381 Howes, E., Stemmann, L., Assailly, C., Irisson, J.-O., Dima, M., Bijma, J., Gattuso, J.-P.: Pteropod time series  
1382 from the North Western Mediterranean (1967-2003): impacts of pH and climate variability. *Mar Ecol Prog Ser*  
1383 531: 193-206, doi: 10.3354/meps11322. 2015.  
1384  
1385 Huang, B., P. W. Thorne, V. F. Banzon, T. Boyer, G. Chepurin, J. H. Lawrimore, M. J. Menne, T. M. Smith, R.  
1386 S. Vose, and H.-M. Zhang: Extended Reconstructed Sea Surface Temperature, version 5 (ERSSTv5): Upgrades,  
1387 validations, and intercomparisons. *J. Climate*, 30, 8179-8205, doi:10.1175/JCLI-D-16-0836.1, 2017  
1388  
1389 IPCC. Changing Ocean, Marine Ecosystems, and Dependent Communities. in *The Ocean and Cryosphere in a*  
1390 *Changing Climate* 447–588 (Cambridge University Press, 2022). doi:10.1017/9781009157964.007. 2022  
1391  
1392 Jiang, Z.-P., Tyrrell, T., Hydes, D. J., Dai, M., and Hartman, S. E.: Variability of alkalinity and the alkalinity-  
1393 salinity relationship in the tropical and subtropical surface ocean, *Global Biogeochem. Cycles*, 28, 729–742,  
1394 doi:10.1002/2013GB004678, 2014.  
1395  
1396 Jiang, L.-Q., Feely, R. A., Wanninkhof, R., Greeley, D., Barbero, L., Alin, S., Carter, B. R., Pierrot, D.,  
1397 Featherstone, C., Hooper, J., Melrose, C., Monacci, N., Sharp, J. D., Shellito, S., Xu, Y.-Y., Kozyr, A., Byrne, R.  
1398 H., Cai, W.-J., Cross, J., Johnson, G. C., Hales, B., Langdon, C., Mathis, J., Salisbury, J., and Townsend, D. W.:  
1399 Coastal Ocean Data Analysis Product in North America (CODAP-NA) – an internally consistent data product for  
1400 discrete inorganic carbon, oxygen, and nutrients on the North American ocean margins. *Earth System Science*  
1401 *Data*, 13(6), 2777–2799. <https://doi.org/10.5194/essd-13-2777-2021>, 2021  
1402  
1403 Jiang, L.-Q., Dunne, J., Carter, B. R., Tjiputra, J. F., Terhaar, J., Sharp, J. D., et al.: Global surface ocean  
1404 acidification indicators from 1750 to 2100. *Journal of Advances in Modeling Earth Systems*, 15,  
1405 e2022MS003563. <https://doi.org/10.1029/2022MS003563> , 2023  
1406  
1407 Jiang, L.Q., Fay, A., Müller, J. D. et al: Synthesis products for ocean carbon chemistry. In prep., 2024.  
1408  
1409 Jing, Y., Li, Y., Xu, Y., and Fan, G.: Influences of the NAO on the North Atlantic CO<sub>2</sub> fluxes in winter and  
1410 summer on the interannual scale. *Advances in Atmospheric Sciences*, 36(11), 1288–1298.  
1411 <https://doi.org/10.1007/s00376-019-8247-2>, 2019  
1412  
1413 Kapsenberg, L., Alliouane, S., Gazeau, F., Mousseau, L., and Gattuso, J.-P.: Coastal ocean acidification and  
1414 increasing total alkalinity in the northwestern Mediterranean Sea, *Ocean Sci.*, 13, 411-426, doi:10.5194/os-13-  
1415 411-2017, 2017.  
1416  
1417 Khatiwala, S., Tanhua, T., Mikaloff Fletcher, S., Gerber, M., Doney, S. C., Graven, H. D., Gruber, N.,  
1418 McKinley, G. A., Murata, A., Ríos, A. F., and Sabine, C. L.: Global ocean storage of anthropogenic carbon,  
1419 *Biogeosciences*, 10, 2169-2191, <https://doi.org/10.5194/bg-10-2169-2013>, 2013.  
1420  
1421 Koffi, U., Lefèvre, N., Kouadio, G., and Boutin, J.: Surface CO<sub>2</sub> parameters and air-sea CO<sub>2</sub> fluxes distribution  
1422 in the eastern equatorial Atlantic Ocean. *J. Marine Systems*, doi:10.1016/j.jmarsys/2010.04.010. 2010.  
1423  
1424 Kwiatkowski, L., Torres, O., Bopp, L., Aumont, O., Chamberlain, M., Christian, J. R., Dunne, J. P., Gehlen, M.,  
1425 Ilyina, T., John, J. G., Lenton, A., Li, H., Lovenduski, N. S., Orr, J. C., Palmieri, J., Santana-Falcón, Y.,  
1426 Schwinger, J., Séférian, R., Stock, C. A., Tagliabue, A., Takano, Y., Tjiputra, J., Toyama, K., Tsujino, H.,  
1427 Watanabe, M., Yamamoto, A., Yool, A., and Ziehn, T.: Twenty-first century ocean warming, acidification,

1428 deoxygenation, and upper-ocean nutrient and primary production decline from CMIP6 model projections,  
1429 Biogeosciences, 17, 3439–3470, <https://doi.org/10.5194/bg-17-3439-2020>, 2020.

1430

1431 Lacoue-Labarthe, T., Nunes, P. A. L. D., Ziveri, P., Cinar, M., Gazeau, F., Hall-Spencer, J. M., Hilmi, N.,  
1432 Moschella, P., Safa, A., Sauzade, D., and Turley, C.: Impacts of ocean acidification in a warming Mediterranean  
1433 Sea: An overview, Regional Studies in Marine Science, 5, 1–11, doi:10.1016/j.rsma.2015.12.005, 2016.

1434

1435 Lagoutte, E., A. Tribollet, S. Bureau, et al., Biogeochemical evidence of flow re-entrainment on the main  
1436 fringing reef of La Reunion Island, Marine Chemistry, <https://doi.org/10.1016/j.marchem.2024.104352>, 2023.

1437

1438 Laika, H. E., Goyet C., Vouve F., Poisson A., and Touratier F. : Interannual properties of the CO<sub>2</sub> system in the  
1439 Southern Ocean south of Australia. Antarctic Science, 21(6), 663-680.  
1440 <https://doi.org/10.1017/S0954102009990319>, 2009

1441

1442 Lan, X., Tans, P. and K.W. Thoning: Trends in globally-averaged CO<sub>2</sub> determined from NOAA Global  
1443 Monitoring Laboratory measurements. Version 2024-08 <https://doi.org/10.15138/9N0H-ZH07> (last access: 14  
1444 August 2024), 2024.

1445

1446 Landschützer, P., Gruber, N., Bakker, D. C. E., Stemmler, I., and Six, K. D.: Strengthening seasonal marine CO<sub>2</sub>  
1447 variations due to increasing atmospheric CO<sub>2</sub>. Nature Climate Change, 8(2), 146–150.  
1448 <https://doi.org/10.1038/s41558-017-0057-x>, 2018

1449

1450 Landschützer, P., Ilyina, T., and Lovenduski, N. S. : Detecting regional modes of variability in observation-  
1451 based surface ocean pCO<sub>2</sub>. Geophysical Research Letters, 46. <https://doi.org/10.1029/2018GL081756>, 2019

1452

1453 Lange, N., Fiedler, B., Álvarez, M., Benoit-Cattin, A., Benway, H., Buttigieg, P. L., Coppola, L., Currie, K.,  
1454 Flecha, S., Gerlach, D. S., Honda, M., Huertas, I. E., Lauvset, S. K., Muller-Karger, F., Körtzinger, A., O'Brien,  
1455 K. M., Ólafsdóttir, S. R., Pacheco, F. C., Rueda-Roa, D., Skjelvan, I., Wakita, M., White, A., and Tanhua, T.:  
1456 Synthesis Product for Ocean Time Series (SPOTS) – a ship-based biogeochemical pilot, Earth Syst. Sci. Data,  
1457 16, 1901–1931, <https://doi.org/10.5194/essd-16-1901-2024>, 2024.

1458

1459 LANSARD Bruno (2014) DICASE cruise, RV Téthys II, <https://doi.org/10.17600/14007100>

1460

1461 Laruelle, G. G., Dürr, H. H., Lauerwald, R., Hartmann, J., Slomp, C. P., Goossens, N., and Regnier, P. A. G.:  
1462 Global multi-scale segmentation of continental and coastal waters from the watersheds to the continental  
1463 margins, Hydrol. Earth Syst. Sci., 17, 2029–2051, <https://doi.org/10.5194/hess-17-2029-2013>, 2013.

1464

1465 Laruelle, G. G. et al. Continental shelves as a variable but increasing global sink for atmospheric carbon dioxide.  
1466 Nat. Commun. 9, 454, DOI: 10.1038/s41467-017-02738-z, 2018

1467

1468 Lauvset, S. K., Lange, N., Tanhua, T., Bittig, H. C., Olsen, A., Kozyr, A., Álvarez, M., Azetsu-Scott, K., Brown,  
1469 P. J., Carter, B. R., Cotrim da Cunha, L., Hoppema, M., Humphreys, M. P., Ishii, M., Jeansson, E., Murata, A.,  
1470 Müller, J. D., Pérez, F. F., Schirnack, C., Steinfeldt, R., Suzuki, T., Ulfso, A., Velo, A., Woosley, R. J., and  
1471 Key, R. M.: The annual update GLODAPv2.2023: the global interior ocean biogeochemical data product, Earth  
1472 Syst. Sci. Data, 16, 2047–2072, <https://doi.org/10.5194/essd-16-2047-2024>, 2024.

1473

1474 Lefèvre, D.: MOOSE (ANTARES), <https://doi.org/10.18142/233>, 2010.

1475

1476 Lefèvre N.: Carbon parameters along a zonal transect. SEANOE. <https://doi.org/10.17882/58575>, 2010.

1477

1478 Lefèvre Nathalie (2017). Carbon parameters in the gulf of Maranhao. SEANOE. <https://doi.org/10.17882/62417>

1479



1480 Lefèvre Nathalie (2018). Carbon parameters in the Western tropical Atlantic. SEANOE.  
1481 <https://doi.org/10.17882/58406>  
1482  
1483 Lefèvre Nathalie (2019). Carbon parameters in the Eastern Tropical Atlantic in 2019. SEANOE.  
1484 <https://doi.org/10.17882/83682>  
1485  
1486 Lefèvre Nathalie (2020). Inorganic carbon and alkalinity in the Eastern tropical Atlantic measured during the  
1487 PIRATA FR-30 cruise in February-March 2020. SEANOE. <https://doi.org/10.17882/90742>  
1488  
1489 Lefèvre Nathalie (2022). Inorganic carbon and alkalinity in the Eastern tropical Atlantic in 2022. SEANOE.  
1490 <https://doi.org/10.17882/92386>  
1491  
1492 Lefèvre, N., Urbano, D.F., Gallois, F., and Diverrès, D.: Impact of physical processes on the seasonal  
1493 distribution of CO<sub>2</sub> in the western tropical Atlantic. *Journal of Geophysical Research* 119,  
1494 doi: 10.1002/2013JC009248. doi: DOI: 10.1002/2013JC009248, 2014  
1495  
1496 Lefèvre, N., Veleda, D., Araujo, M., Caniaux, G.: Variability and trends of carbon parameters at a time series in  
1497 the eastern tropical Atlantic. *Tellus B*, Co-Action Publishing, 68, pp.30305. 10.3402/tellusb.v68.30305. 2016.  
1498  
1499 Lefèvre N., da Silva Dias F. J., de Torres A. R., Noriega C., Araujo M., de Castro A. C. L., Rocha C., Jiang S.,  
1500 Ibánhez J. S. P.: A source of CO<sub>2</sub> to the atmosphere throughout the year in the Maranhense continental shelf  
1501 (2°30'S, Brazil). *Continental Shelf Research*, 141, 38-50. <https://doi.org/10.1016/j.csr.2017.05.004>, 2017a  
1502  
1503 Lefèvre N., Flores Montes M., Gaspar F. L., Rocha C., Jiang S., De Araújo M. C., Ibánhez J. S. P. : Net  
1504 Heterotrophy in the Amazon Continental Shelf Changes Rapidly to a Sink of CO<sub>2</sub> in the Outer Amazon Plume.  
1505 *Frontiers in Marine Science*, 4, -. <https://doi.org/10.3389/fmars.2017.00278>, 2017b  
1506  
1507 Lefèvre, N., Mejia, C., Khvorostyanov, D., Beaumont, L., and Koffi, U.: Ocean Circulation Drives the  
1508 Variability of the Carbon System in the Eastern Tropical Atlantic. *Oceans*, 2021, 2, 126–148.  
1509 <https://doi.org/10.3390/oceans2010008>, 2021.  
1510  
1511 Lefèvre, N., Veleda, D., Hartman, S.E.: Outgassing of CO<sub>2</sub> dominates in the coastal upwelling off the northwest  
1512 African coast, *Deep-Sea Research Part I*, doi: <https://doi.org/10.1016/j.dsr.2023.104130>, 2023  
1513  
1514 Lefèvre, N., Veleda, D. and Beaumont; L.: Trends and drivers of CO<sub>2</sub> parameters, from 2006 to 2021, at a time-  
1515 series station in the Eastern Tropical Atlantic (6°S, 10°W). *Front. Mar. Sci.* 11:1299071. doi:  
1516 10.3389/fmars.2024.1299071, 2024  
1517  
1518 Leseurre, C.: Mécanismes de contrôle de l'absorption de CO<sub>2</sub> anthropique et de l'acidification des eaux dans les  
1519 océans Atlantique Nord et Austral. PhD Thesis, Sorbonne Univ., 270 pp. <https://theses.hal.science/tel-04028410>,  
1520 2022  
1521  
1522 Leseurre, C., Lo Monaco, C., Reverdin, G., Metzl, N., Fin, J., Olafsdottir, S., and Racapé, V.: Ocean carbonate  
1523 system variability in the North Atlantic Subpolar surface water (1993–2017), *Biogeosciences*, 17, 2553–2577,  
1524 <https://doi.org/10.5194/bg-17-2553-2020>, 2020  
1525  
1526 Leseurre, C., Lo Monaco, C., Reverdin, G., Metzl, N., Fin, J., Mignon, C., and Benito, L.: Summer trends and  
1527 drivers of sea surface fCO<sub>2</sub> and pH changes observed in the southern Indian Ocean over the last two decades  
1528 (1998–2019), *Biogeosciences*, 19, 2599–2625, <https://doi.org/10.5194/bg-19-2599-2022>, 2022.  
1529  
1530 Li, X., et al.: The source and accumulation of anthropogenic carbon in the U.S. East Coast, *Sci. Adv.* 10,  
1531 eadl3169, DOI: 10.1126/sciadv.adl3169, 2024  
1532

1533 LO MONACO Claire, METZL Nicolas (2019) VT 163 / OISO-29 cruise, RV Marion Dufresne,  
1534 <https://doi.org/10.17600/18000972>  
1535  
1536 LO MONACO Claire (2020) OISO-30 cruise, RV Marion Dufresne, <https://doi.org/10.17600/18000679>  
1537  
1538 LO MONACO Claire, JEANDEL Catherine, PLANQUETTE Hélène (2021) OISO-31 cruise, RV Marion  
1539 Dufresne, <https://doi.org/10.17600/18001254>  
1540  
1541 Lo Monaco, Claire; Metzl, Nicolas; Fin, Jonathan (2022). Sea surface measurements of dissolved inorganic  
1542 carbon (DIC), total alkalinity (TALK), temperature and salinity during the R/V Marion-Dufresne Ocean Indien  
1543 Service d'Observations - 29 (OISO-29) cruise (EXPOCODE 35MV20190106) in the Indian Ocean from 2019-  
1544 01-06 to 2019-02-09 (NCEI Accession 0252612). NOAA National Centers for Environmental Information.  
1545 Dataset. <https://doi.org/10.25921/8ajx-za24>. Accessed 14-Aug-2024.  
1546  
1547 Lo Monaco, Claire; Metzl, Nicolas (2023). Sea surface measurements of dissolved inorganic carbon (DIC), total  
1548 alkalinity (TALK), temperature and salinity during the R/V Marion-Dufresne Ocean Indien Service  
1549 d'Observations - 30 (OISO-30) cruise (EXPOCODE 35MV20200106) in the Indian Ocean from 2020-01-06 to  
1550 2020-02-01 (NCEI Accession 0280937). NOAA National Centers for Environmental Information. Dataset.  
1551 <https://doi.org/10.25921/n2g0-pp38>. Accessed 14-Aug-2024  
1552  
1553 Lo Monaco, Claire; Metzl, Nicolas; Fin, Jonathan (2023). Sea surface measurements of dissolved inorganic  
1554 carbon (DIC), total alkalinity (TALK), temperature and salinity during the R/V Marion-Dufresne Ocean  
1555 Indien Service d'Observations - 31 (OISO-31) cruise (EXPOCODE 35MV20210113) in the Indian Ocean  
1556 from 2021-01-14 to 2021-03-04 (NCEI Accession 0280946). NOAA National Centers for Environmental  
1557 Information. Dataset. <https://doi.org/10.25921/7sb2-k852>. Accessed 14-Aug-2024  
1558  
1559 Mathis, M., Lacroix, F., Hagemann, S. et al.: Enhanced CO<sub>2</sub> uptake of the coastal ocean is dominated by  
1560 biological carbon fixation. *Nat. Clim. Chang.* <https://doi.org/10.1038/s41558-024-01956-w>, 2024  
1561  
1562 Maugendre, L., J.-P. Gattuso, J. Louis, A. de Kluijver, S. Marro, K. Soetaert, F. Gazeau: Effect of ocean  
1563 warming and acidification on a plankton community in the NW Mediterranean Sea, *ICES Journal of Marine*  
1564 *Science*, Volume 72, Issue 6, July/August 2015, Pages 1744–1755, <https://doi.org/10.1093/icesjms/fsu161>, 2015  
1565  
1566 Mercier, H., Lherminier, P., Sarafanov, A., Gaillard, F., Daniault, N., Desbruyères, D., Falina, A., Ferron, B.,  
1567 Huck, T., and Thierry, V.: Variability of the meridional overturning circulation at the Greenland-Portugal Ovide  
1568 section from 1993 to 2010. *Progress in Oceanography*, 132, 250-261, [doi:10.1016/j.pocean.2013.11.001](https://doi.org/10.1016/j.pocean.2013.11.001). 2015  
1569  
1570 Mercier, H., Desbruyères, D., Lherminier, P., Velo, A., Carracedo, L., Fontela, M., and Pérez, F. F.: New  
1571 insights into the eastern subpolar North Atlantic meridional overturning circulation from OVIDE, *Ocean Sci.*,  
1572 20, 779–797, <https://doi.org/10.5194/os-20-779-2024>, 2024.  
1573  
1574 Metzl, N., Brunet, C., Jabaud-Jan, A., Poisson, A., and Schauer, B.: Summer and winter air-sea CO<sub>2</sub> fluxes in  
1575 the Southern Ocean *Deep Sea Res I*, 53, 1548-1563, doi:10.1016/j.dsr.2006.07.006. 2006.  
1576  
1577 Metzl, N., Corbière, A., Reverdin, G., Lenton, A., Takahashi, T., Olsen, A., Johannessen, T., Pierrot, D.,  
1578 Wanninkhof, R., Ólafsdóttir, S. R., Ólafsson, J., and Ramonet, M.: Recent acceleration of the sea surface fCO<sub>2</sub>  
1579 growth rate in the North Atlantic subpolar gyre (1993-2008) revealed by winter observations, *Global*  
1580 *Biogeochem. Cycles*, 24, GB4004, doi:10.1029/2009GB003658, 2010.  
1581  
1582 Metzl, N., and Lo Monaco, C.: OISO - OCÉAN INDIEN SERVICE D'OBSERVATION,  
1583 <https://doi.org/10.18142/228>, 1998.  
1584

1585 Metzl, N., Lo Monaco, C., Leseurre, C., Ridame, C., Fin, J., Mignon, C., Gehlen, M., and Chau, T. T. T.: The  
1586 impact of the South-East Madagascar Bloom on the oceanic CO<sub>2</sub> sink, *Biogeosciences*, 19, 1451–1468,  
1587 <https://doi.org/10.5194/bg-19-1451-2022>, 2022  
1588

1589 Metzl Nicolas, Fin Jonathan, Lo Monaco Claire, Mignon Claude, Alliouane Samir, Antoine David, Bourdin  
1590 Guillaume, Boutin Jacqueline, Bozec Yann, Conan Pascal, Coppola Laurent, Douville Eric, Durrieu de Madron  
1591 Xavier, Gattuso Jean-Pierre, Gazeau Frédéric, Golbol Melek, Lansard Bruno, Lefèvre Dominique, Lefèvre  
1592 Nathalie, Lombard Fabien, Louanchi Férial, Merlivat Liliane, Olivier Léa, Petrenko Anne, Petton Sébastien,  
1593 Pujo-Pay Mireille, Rabouille Christophe, Reverdin Gilles, Ridame Céline, Tribollet Aline, Vellucci Vincenzo,  
1594 Wagener Thibaut, Wimart-Rousseau Cathy: SNAPO-CO<sub>2</sub> data-set: A synthesis of total alkalinity and total  
1595 dissolved inorganic carbon observations in the global ocean (1993-2022). *SEANOE*.  
1596 <https://doi.org/10.17882/95414>, 2023  
1597

1598 Metzl, N., Fin, J., Lo Monaco, C., Mignon, C., Alliouane, S., Antoine, D., Bourdin, G., Boutin, J., Bozec, Y.,  
1599 Conan, P., Coppola, L., Díaz, F., Douville, E., Durrieu de Madron, X., Gattuso, J.-P., Gazeau, F., Golbol, M.,  
1600 Lansard, B., Lefèvre, D., Lefèvre, N., Lombard, F., Louanchi, F., Merlivat, L., Olivier, L., Petrenko, A., Petton,  
1601 S., Pujo-Pay, M., Rabouille, C., Reverdin, G., Ridame, C., Tribollet, A., Vellucci, V., Wagener, T., and Wimart-  
1602 Rousseau, C.: A synthesis of ocean total alkalinity and dissolved inorganic carbon measurements from 1993 to  
1603 2022: the SNAPO-CO<sub>2</sub>-v1 dataset, *Earth Syst. Sci. Data*, 16, 89–120, <https://doi.org/10.5194/essd-16-89-2024>,  
1604 2024a  
1605

1606 Metzl, N., Lo Monaco, C., Leseurre, C., Ridame, C., Reverdin, G., Chau, T. T. T., Chevallier, F., and Gehlen,  
1607 M.: Anthropogenic CO<sub>2</sub>, air–sea CO<sub>2</sub> fluxes, and acidification in the Southern Ocean: results from a time-series  
1608 analysis at station OISO-KERFIX (51° S–68° E), *Ocean Sci.*, 20, 725–758, [https://doi.org/10.5194/os-20-725-](https://doi.org/10.5194/os-20-725-2024)  
1609 2024, 2024b.  
1610

1611 Metzl, N., ~~C.~~ Lo Monaco, ~~G.C.~~, Barut, ~~G.~~, and ~~J.F.~~ TERNON, ~~J.F.~~: Contrasting trends of the ocean CO<sub>2</sub> sink and  
1612 pH in the Agulhas current system and the Mozambique Basin, South-Western Indian Ocean (1963-2023). *Sub*  
1613 *DSRH Deep Sea Res.*, special issue IIOE-2, *in rev.*, 2024c  
1614

1615 Metzl Nicolas, Fin Jonathan, Lo Monaco Claire, Mignon Claude, Alliouane Samir, Bombled Bruno, Boutin  
1616 Jacqueline, Bozec Yann, Comeau Steeve, Conan Pascal, Coppola Laurent, Cuet Pascale, Ferreira Eva, Gattuso  
1617 Jean-Pierre, Gazeau Frédéric, Goyet Catherine, Grossteffan Emilie, Lansard Bruno, Lefèvre Dominique, Lefèvre  
1618 Nathalie, Leseurre Coraline, Lombard Fabien, Petton Sébastien, Pujo-Pay Mireille, Rabouille Christophe,  
1619 Reverdin Gilles, Ridame Céline, Rimmelin-Mauray Peggy, TERNON Jean-François, Touratier Franck, Tribollet  
1620 Aline, Wagener Thibaut, Wimart-Rousseau Cathy ~~(2024)~~: An updated synthesis of ocean total alkalinity and  
1621 dissolved inorganic carbon measurements from 1993 to 2023: the SNAPO-CO<sub>2</sub>-v2 dataset. *SEANOE*.  
1622 <https://doi.org/10.17882/102337SEANOE>, <https://doi.org/10.17882/102337>, 2024d  
1623

1624 MICHEL Elisabeth, VIVIER Frédéric ~~(2016)~~: STEP 2016 cruise, RV L'Atalante,  
1625 <https://doi.org/10.17600/16000900> <https://doi.org/10.17600/16000900>, 2016  
1626

1627 Mu, L., Gomes, H. do R., Burns, S. M., Goes, J. I., Coles, V. J., Rezende, C. E., et al.: Temporal Variability of  
1628 Air-Sea CO<sub>2</sub> flux in the Western Tropical North Atlantic Influenced by the Amazon River Plume. *Global*  
1629 *Biogeochemical Cycles*, 35(6). <https://doi.org/10.1029/2020GB006798>, 2021  
1630

1631 Munro, D. R., Lovenduski, N. S., Takahashi, T., Stephens, B. B., Newberger, T., and Sweeney, C.: Recent  
1632 evidence for a strengthening CO<sub>2</sub> sink in the Southern Ocean from carbonate system measurements in the Drake  
1633 Passage (2002–2015), *Geophys. Res. Lett.*, 42, 7623–7630, <https://doi.org/10.1002/2015GL065194>, 2015.  
1634

1635 Müller, J. D., Gruber, N., Carter, B., Feely, R., Ishii, M., Lange, N., et al.: Decadal trends in the oceanic storage  
1636 of anthropogenic carbon from 1994 to 2014. *AGU Advances*, 4, e2023AV000875.  
1637 <https://doi.org/10.1029/2023AV000875>, 2023

1638  
1639 Newton, J.A., Feely, R. A., Jewett, E. B., Williamson, P. and Mathis, J.: Global Ocean Acidification Observing  
1640 Network: Requirements and Governance Plan. Second Edition, GOA-ON,  
1641 <https://www.iaea.org/sites/default/files/18/06/goa-on-second-edition-2015.pdf>, 2015.  
1642  
1643 Olafsson, J., Olafsdottir, S. R., Benoit-Cattin, A., and Takahashi, T.: The Irminger Sea and the Iceland Sea time  
1644 series measurements of sea water carbon and nutrient chemistry 1983–2008, *Earth Syst. Sci. Data*, 2, 99–104,  
1645 <https://doi.org/10.5194/essd-2-99-2010>, 2010.  
1646  
1647 Olivier, L., Boutin, J., Reverdin, G., Lefèvre, N., Landschützer, P., Speich, S., Karstensen, J., Labaste, M.,  
1648 Noisel, C., Ritschel, M., Steinhoff, T., and Wanninkhof, R.: Wintertime process study of the North Brazil  
1649 Current rings reveals the region as a larger sink for CO<sub>2</sub> than expected, *Biogeosciences*, 19, 2969–2988,  
1650 <https://doi.org/10.5194/bg-19-2969-2022>, 2022.  
1651  
1652 Olsen, A., Key, R. M., van Heuven, S., Lauvset, S. K., Velo, A., Lin, X., Schirnack, C., Kozyr, A., Tanhua, T.,  
1653 Hoppema, M., Jutterström, S., Steinfeldt, R., Jeansson, E., Ishii, M., Pérez, F. F., and Suzuki, T.: The Global  
1654 Ocean Data Analysis Project version 2 (GLODAPv2) – an internally consistent data product for the world ocean,  
1655 *Earth Syst. Sci. Data*, 8, 297–323, <https://doi.org/10.5194/essd-8-297-2016>, 2016.  
1656  
1657 Oudot, C., Ternon, J. F., and Lecomte, J.: Measurements of atmospheric and oceanic CO<sub>2</sub> in the tropical Atlantic:  
1658 10 years after the 1982-1984 FOCAL cruises. *Tellus B: Chemical and Physical Meteorology*, 47(1–2), 70–85.  
1659 <https://doi.org/10.3402/tellusb.v47i1-2.16032>, 1995  
1660  
1661 Padin, X. A., Velo, A., and Pérez, F. F.: ARIOS: a database for ocean acidification assessment in the Iberian  
1662 upwelling system (1976–2018), *Earth Syst. Sci. Data*, 12, 2647–2663, [https://doi.org/10.5194/essd-12-2647-](https://doi.org/10.5194/essd-12-2647-2020)  
1663 2020, 2020.  
1664  
1665 Palacio-Castro, A. M., Enochs, I. C., Besemer, N., Boyd, A., Jankulak, M., Kolodziej, G., et al.: Coral reef  
1666 carbonate chemistry reveals interannual, seasonal, and spatial impacts on ocean acidification off Florida. *Global*  
1667 *Biogeochemical Cycles*, 37, e2023GB007789. <https://doi.org/10.1029/2023GB007789>, 2023  
1668  
1669 Pardo, P. C., Tilbrook, B., Langlais, C., Trull, T. W., and Rintoul, S. R.: Carbon uptake and biogeochemical  
1670 change in the Southern Ocean, south of Tasmania. *Biogeosciences*, 14(22), 5217–5237.  
1671 <https://doi.org/10.5194/bg-14-5217-2017>, 2017.  
1672  
1673 Pérez, F. F., Becker, M., Goris, N., Gehlen, M., López-Mozos, M., Tjiputra, J., et al.: An assessment of CO<sub>2</sub>  
1674 storage and sea-air fluxes for the Atlantic Ocean and Mediterranean Sea between 1985 and 2018. *Global*  
1675 *Biogeochemical Cycles*, 38, e2023GB007862. <https://doi.org/10.1029/2023GB007862>, 2024  
1676  
1677 Petton, S., Pernet, F., Le Roy, V., Huber, M., Martin, S., Macé, É., Bozec, Y., Loisel, S., Rimmelin Maury, P.,  
1678 Grossteffan, É., Repecaud, M., Quemener, L., Retho, M., Manac'h, S., Papin, M., Pineau, P., Lacoue-Labarthe,  
1679 T., Deborde, J., Costes, L., Polsenaere, P., Rigouin, L., Benhamou, J., Gouriou, L., Lequeux, J., Labourdette, N.,  
1680 Savoye, N., Messiaen, G., Foucault, E., Ouisse, V., Richard, M., Lagarde, F., Voron, F., Kempf, V., Mas, S.,  
1681 Giannecchini, L., Vidussi, F., Mostajir, B., Leredde, Y., Alliouane, S., Gattuso, J.-P., and Gazeau, F.: French  
1682 coastal network for carbonate system monitoring: the CocoriCO<sub>2</sub> dataset, *Earth Syst. Sci. Data*, 16, 1667–1688,  
1683 <https://doi.org/10.5194/essd-16-1667-2024>, 2024.  
1684  
1685 Petton Sébastien, Pernet Fabrice, Le Roy Valerian, Huber Matthias, Martin Sophie, Mace Eric, Bozec Yann,  
1686 Loisel Stéphane, Rimmelin-Maury Peggy, Grossteffan Emilie, Repecaud Michel, Quémener Loïc, Retho  
1687 Michael, Manach Soazig, Papin Mathias, Pineau Philippe, Lacoue-Labarthe Thomas, Deborde Jonathan, Costes  
1688 Louis, Polsenaere Pierre, Rigouin Loic, Benhamou Jeremy, Gouriou Laure, Lequeux Joséphine, Labourdette  
1689 Nathalie, Savoye Nicolas, Messiaen Gregory, Foucault Elodie, Lagarde Franck, Richard Marion, Ouisse  
1690 Vincent, Voron Florian, Mas Sébastien, Giannecchini Léa, Vidussi Francesca, Mostajir Behzad, Leredde Yann,

1691 Kempf Valentin, Alliouane Samir, Gattuso Jean-Pierre, Gazeau Frédéric ~~(2023)~~; French coastal carbonate  
1692 dataset from the CocoriCO2 project. SEANOE. <https://doi.org/10.17882/96982><https://doi.org/10.17882/96982>,  
1693 <https://doi.org/10.17882/96982>, 2023  
1694  
1695 Poisson, A., Culkin, F., and Ridout, P.: Intercomparison of CO2 measurements. Deep Sea Research Part A.  
1696 Oceanographic Research Papers, 37, 10, 1647-1650, [https://doi.org/10.1016/0198-0149\(90\)90067-6](https://doi.org/10.1016/0198-0149(90)90067-6), 1990.  
1697  
1698 Pozzato, L., Rassmann, J., Lansard, B., Dumoulin, J.-P., Van Breugel, P., and Rabouille, C.: Origin of  
1699 remineralized organic matter in sediments from the Rhone River prodelta (NW Mediterranean) traced by Delta  
1700 C-14 and delta C-13 signatures of pore water DIC. Progress In Oceanography, 163, 112-122.  
1701 <https://doi.org/10.1016/j.pocean.2017.05.008>, 2018  
1702  
1703 RABOUILLE Christophe (2010) MESURHOBENT 1 cruise, RV Téthys II, <https://doi.org/10.17600/10450020>  
1704  
1705 RABOUILLE Christophe (2013) CARBODELTA cruise, RV Téthys II, <https://doi.org/10.17600/13450060>  
1706  
1707 RABOUILLE Christophe (2018) MISSRHODIA2 cruise, RV Téthys II, <https://doi.org/10.17600/18000473>  
1708  
1709 RABOUILLE Christophe, BOURRIN François, BASSETTI Maria-Angela (2022) DELTARHONE-1 cruise, RV  
1710 Téthys II, <https://doi.org/10.17600/18002027>  
1711  
1712 Regnier, P., Friedlingstein, P., Ciais, P., Mackenzie, F. T., Gruber, N., et al: Anthropogenic perturbation of the  
1713 carbon fluxes from land to ocean. Nat. Geosci. 6:597–607-, 2013.  
1714  
1715 Resplandy, L., Hogikyan, A., Müller, J. D., Najjar, R. G., Bange, H. W., Bianchi, D., et al.: A synthesis of global  
1716 coastal ocean greenhouse gas fluxes. Global Biogeochemical Cycles, 38, e2023GB007803.  
1717 <https://doi.org/10.1029/2023GB007803>, 2024  
1718  
1719 Revelle, R., and Suess, H. E.: Carbon dioxide exchange between atmosphere and ocean and the question of an  
1720 increase of atmospheric CO2 during the past decades. Tellus 9, 18–27. doi:10.1111/j.2153-  
1721 3490.1957.tb01849.x., 1957.  
1722  
1723 Reverdin, G., Metzl, N., Olafsdottir, S., Racapé, V., Takahashi, T., Benetti, M., Valdimarsson, H., Benoit-Cattin,  
1724 A., Danielsen, M., Fin, J., Naamar, A., Pierrot, D., Sullivan, K., Bringas, F., and Goni, G.: SURATLANT: a  
1725 1993–2017 surface sampling in the central part of the North Atlantic subpolar gyre, Earth Syst. Sci. Data, 10,  
1726 1901-1924, <https://doi.org/10.5194/essd-10-1901-2018>, 2018.  
1727  
1728 Reverdin, G., Metzl, N., Olafsdottir, S., Racapé, V., Takahashi, T., Benetti, M., Valdimarsson, H., Quay, P. D.,  
1729 Benoit-Cattin, A., Danielsen, M., Fin, J., Naamar, A., Pierrot, D., Sullivan, K., Bringas, F., Goni, G., Becker M.,  
1730 Leseurre C., and Olsen A.: SURATLANT: a surface dataset in the central part of the North Atlantic subpolar  
1731 gyre. SEANOE. <https://doi.org/10.17882/54517>, 2023.  
1732  
1733 Rodgers, K. B., Schwinger, J., Fassbender, A. J., Landschützer, P., Yamaguchi, R., Frenzel, H., et al.: Seasonal  
1734 variability of the surface ocean carbon cycle: A synthesis. Global Biogeochemical Cycles, 37, e2023GB007798.  
1735 <https://doi.org/10.1029/2023GB007798>, 2023  
1736  
1737 Roobaert, A., Resplandy, L., Laruelle, G. G., Liao, E., and Regnier, P. : Unraveling the physical and biological  
1738 controls of the global coastal CO2 sink. Global Biogeochemical Cycles, 38, e2023GB007799.  
1739 <https://doi.org/10.1029/2023GB007799>, 2024a  
1740  
1741 Roobaert, A., Regnier, P., Landschützer, P., and Laruelle, G. G.: A novel sea surface pCO2-product for the  
1742 global coastal ocean resolving trends over 1982–2020, Earth Syst. Sci. Data, 16, 421–441,  
1743 <https://doi.org/10.5194/essd-16-421-2024>, 2024b.

1744  
1745 Sarma, V. V. S. S., Krishna, M. S., Paul, Y. S., and Murty, V. S. N.: Observed changes in ocean acidity and  
1746 carbon dioxide exchange in the coastal bay of Bengal—A link to air pollution. *Tellus B: Chemical and Physical*  
1747 *Meteorology*, 67(1), 24638. <https://doi.org/10.3402/tellusb.v67.24638>, 2015  
1748  
1749 Sarma, V. V. S. S., Sridevi, B., Metzl, N., Patra, P. K., Lachkar, Z., Chakraborty, K., et al. : Air-sea fluxes of  
1750 CO<sub>2</sub> in the Indian Ocean between 1985 and 2018: A synthesis based on observation-based surface CO<sub>2</sub>, hindcast  
1751 and atmospheric inversion models. *Global Biogeochemical Cycles*, 37, e2023GB007694.  
1752 <https://doi.org/10.1029/2023GB007694>, 2023  
1753  
1754 Sarmiento, J.L., Johnson, K.S., Arteaga, L.A., Bushinsky, S.M., Cullen, H.M., Gray, A.R., Hotinski, R.M.,  
1755 Maurer, T.L., Mazloff, M.R., Riser, S.C., Russell, J.L., Schofield, O.M., Talley, L.D., The Southern Ocean  
1756 Carbon and Climate Observations and Modeling (SOCCOM) project: A review, *Progress in Oceanography*, doi:  
1757 <https://doi.org/10.1016/j.pocean.2023.103130>, 2023  
1758  
1759 Schlitzer, R.: Ocean Data View, Ocean Data View, <http://odv.awi.de> (last access: 13 March 2019), 2018.  
1760  
1761 Schneider, A., Wallace, D. W. R., and Körtzinger, A.: Alkalinity of the Mediterranean Sea, *Geophys. Res. Lett.*,  
1762 34, L15608, doi:10.1029/2006GL028842, 2007.  
1763  
1764 Schuster, U., McKinley, G. A., Bates, N., Chevallier, F., Doney, S. C., Fay, A. R., González-Dávila, M., Gruber,  
1765 N., Jones, S., Krijnen, J., Landschützer, P., Lefèvre, N., Manizza, M., Mathis, J., Metzl, N., Olsen, A., Rios, A.  
1766 F., Rödenbeck, C., Santana-Casiano, J. M., Takahashi, T., Wanninkhof, R., and Watson, A. J.: An assessment of  
1767 the Atlantic and Arctic sea–air CO<sub>2</sub> fluxes, 1990–2009, *Biogeosciences*, 10, 607–627,  
1768 <https://doi.org/10.5194/bg-10-607-2013>, 2013.  
1769  
1770 Shadwick, E., Rintoul, S., Tilbrook, B., Williams, G., Young, N., Fraser, A. D., et al.: Glacier tongue calving  
1771 reduced dense water formation and enhanced carbon uptake. *Geophysical Research Letters*, 40(5), 904–909.  
1772 <https://doi.org/10.1002/grl.50178>, 2013  
1773  
1774 Shadwick, E. H., B. Tilbrook, and G. D. Williams: Carbonate chemistry in the Mertz Polynya (East Antarctica):  
1775 Biological and physical modification of dense water outflows and the export of anthropogenic CO<sub>2</sub>, *J. Geophys.*  
1776 *Res. Oceans*, 119, 1–14, doi:10.1002/2013JC009286, 2014  
1777  
1778 Shadwick, E. H., T. W. Trull, B. Tilbrook, A. J. Sutton, E. Schulz, and C. L. Sabine: Seasonality of biological  
1779 and physical controls on surface ocean CO<sub>2</sub> from hourly observations at the Southern Ocean Time Series site  
1780 south of Australia, *Global Biogeochem. Cycles*, 29, 223–238, doi:10.1002/2014GB004906, 2015  
1781  
1782 Shadwick, E. H., Wynn-Edwards, C. A., Matear, R. J., Jansen, P., Schulz, E. and Sutton, A. J.: Observed  
1783 amplification of the seasonal CO<sub>2</sub> cycle at the Southern Ocean Time Series. *Front. Mar. Sci.* 10:1281854. doi:  
1784 10.3389/fmars.2023.1281854, 2023  
1785  
1786 Siddiqui, A. H., Haine, T. W. N., Nguyen, A. T., and Buckley, M. W.: Controls on upper ocean salinity  
1787 variability in the eastern subpolar North Atlantic during 1992–2017. *Journal of Geophysical*  
1788 *Research: Oceans*, 129, e2024JC020887. <https://doi.org/10.1029/2024JC020887>, 2024  
1789  
1790 Sridevi, B., and Sarma, V. V. S. S.: Role of river discharge and warming on ocean acidification and pco<sub>2</sub> levels  
1791 in the Bay of Bengal. *Tellus B: Chemical and Physical Meteorology*, 73 (1), 1–20., DOI:  
1792 10.1080/16000889.2021.1971924, 2021  
1793  
1794 [Sutton, A.J., Battisti, R., Carter, B., Evans, W., Newton, J., Alin, S., Bates, N.R., Cai, W.-J., Currie, K., Feely,](#)  
1795 [R.A., Sabine, C., Tanhua, T., Tilbrook, B., and Wanninkhof, R.: Advancing best practices for assessing trends](#)

1796 | [of ocean acidification time series. \*Frontiers in Marine Science\*, 9: 1045667. doi: 10.3389/fmars.2022.1045667,](#)  
1797 | [2022](#)  
1798 |  
1799 | Takahashi, T., Sutherland, S. C., Wanninkhof, R., Sweeney, C., Feely, R. A., Chipman, D. W., Hales, B.,  
1800 | Friederich, G., Chavez, F., Sabine, C., Watson, A. J., Bakker, D. C., Schuster, U., Metzl, N., Yoshikawa-Inoue,  
1801 | H., Ishii, M., Midorikawa, T., Nojiri, Y., Körtzinger, A., Steinhoff, T., Hoppema, M., Olafsson, J., Arnarson, T.  
1802 | S., Tilbrook, B., Johannessen, T., Olsen, A., Bellerby, R., Wong, C., Delille, B., Bates, N., and de Baar, H. J.:  
1803 | Climatological mean and decadal change in surface ocean pCO<sub>2</sub>, and net sea air CO<sub>2</sub> flux over the global  
1804 | oceans. *Deep-Sea Res. II*, 56 (8-10), 554–577, <http://dx.doi.org/10.1016/j.dsr2.2008.12.009>. 2009.  
1805 |  
1806 | Takahashi, T., Sutherland, S. C., Chipman, D. W., Goddard, J. G., Ho, C., Newberger, T., Sweeney, C. and  
1807 | Munro, D. R.: Climatological distributions of pH, pCO<sub>2</sub>, total CO<sub>2</sub>, alkalinity, and CaCO<sub>3</sub> saturation in the  
1808 | global surface ocean, and temporal changes at selected locations. *Marine Chemistry*, 164, 95–125,  
1809 | doi:10.1016/j.marchem.2014.06.004. 2014.  
1810 |  
1811 | TERNON, J.-F., OUDOT, C., DESSIER, A., DIVERRES, D.: A seasonal tropical sink for atmospheric CO<sub>2</sub> in the Atlantic  
1812 | ocean: the role of the Amazon River discharge, *Marine Chemistry*, Volume 68, Issue 3, Pages 183-201,  
1813 | [https://doi.org/10.1016/S0304-4203\(99\)00077-8](https://doi.org/10.1016/S0304-4203(99)00077-8), 2000  
1814 |  
1815 | TESTOR Pierre, COPPOLA Laurent, BOSSE Anthony (2021) MOOSE-GE 2021 cruise, RV Thalassa,  
1816 | <https://doi.org/10.17600/18001333>  
1817 |  
1818 | TESTOR Pierre, COPPOLA Laurent, BOSSE Anthony (2022) MOOSE-GE 2022 cruise, RV Pourquoi pas ?,  
1819 | <https://doi.org/10.17600/18001854>  
1820 |  
1821 | TESTOR Pierre, DURRIEU de MADRON Xavier (2023) MOOSE-GE 2023 cruise, RV Thalassa,  
1822 | <https://doi.org/10.17600/18002686>  
1823 |  
1824 | Thomas, H., Prowe, A. E. F., Lima, I. D., Doney, S. C., Wanninkhof, R., Greatbatch, R. J., Schuster, U. and  
1825 | Corbière, A.: Changes in the North Atlantic Oscillation influence CO<sub>2</sub> uptake in the North Atlantic over the past  
1826 | 2 decades, *Global Biogeochemical Cycles*, 22(4), doi:10.1029/2007GB003167, 2008  
1827 |  
1828 | Tilbrook, B., Jewett, E. B., DeGrandpre, M. D., Hernandez-Ayon, J. M., Feely, R. A., Gledhill, D. K., Hansson,  
1829 | L., Isensee, K., Kurz, M. L., Newton, J. A., Siedlecki, S. A., Chai, F., Dupont, S., Graco, M., Calvo, E., Greeley,  
1830 | D., Kapsenberg, L., Lebec, M., Pelejero, C., Schoo, K. L., and Telszewski, M.: An Enhanced Ocean  
1831 | Acidification Observing Network: From People to Technology to Data Synthesis and Information Exchange.  
1832 | *Frontiers in Marine Science*, 6, 337, DOI:10.3389/fmars.2019.00337, 2019.  
1833 |  
1834 | TOURATIER Franck, POISSON Alain (1990) MINERVE, <https://doi.org/10.18142/128>  
1835 |  
1836 | Touratier, F., and Goyet, C.: Decadal evolution of anthropogenic CO<sub>2</sub> in the north western Mediterranean Sea  
1837 | from the mid-1990's to the mid-2000's. *Deep Sea Research Part I*.doi:10.1016/j.dsr.2009.05.015, 2009.  
1838 |  
1839 | Ulses, C., Estournel, C., Fourier, M., Coppola, L., Kessouri, F., Lefèvre, D., and Marsaleix, P.: Oxygen budget  
1840 | of the north-western Mediterranean deep- convection region, *Biogeosciences*, 18, 937–960,  
1841 | <https://doi.org/10.5194/bg-18-937-2021>, 2021.  
1842 |  
1843 | Ulses, C., Estournel, C., Marsaleix, P., Soetaert, K., Fourier, M., Coppola, L., Lefèvre, D., Touratier, F., Goyet,  
1844 | C., Guglielmi, V., Kessouri, F., Testor, P., and Durrieu de Madron, X.: Seasonal dynamics and annual budget of  
1845 | dissolved inorganic carbon in the northwestern Mediterranean deep-convection region, *Biogeosciences*, 20,  
1846 | 4683–4710, <https://doi.org/10.5194/bg-20-4683-2023>, 2023.  
1847 |

1848 UNESCO: Intercomparison of total alkalinity and total inorganic carbon determinations in seawater. UNESCO  
1849 Tech. Pap. Mar. Sci. 59., 1990  
1850  
1851 UNESCO: Reference materials for oceanic carbon dioxide measurements. UNESCO Tech. Pap. Mar. Sci. 60.,  
1852 1991  
1853  
1854 United Nations. The Sustainable Development Goals 2020, 68pp. <https://unstats.un.org/sdgs/report/2020/>, 2020  
1855  
1856 Vance, J. M., Currie, K., Suanda, S. H. and Law, C. S.: Drivers of seasonal to decadal mixed layer carbon cycle  
1857 variability in subantarctic water in the Munida Time Series. Front. Mar. Sci. 11:1309560. doi:  
1858 10.3389/fmars.2024.1309560, 2024  
1859  
1860 VERNEY Romaric, RABOUILLE Christophe (2012) MERMEX-ACCESS cruise, RV Téthys II,  
1861 <https://doi.org/10.17600/12450070>  
1862  
1863 VIVIER Frédéric, WAELBROECK Claire, MICHEL Elisabeth (2016) NEXT STEP,  
1864 <https://doi.org/10.18142/338>  
1865  
1866 VERNEY Romaric, RABOUILLE Christophe (2012) MERMEX-ACCESS cruise, RV Téthys II,  
1867 <https://doi.org/10.17600/12450070>  
1868  
1869 von Schuckmann, K., Minière, A., Gues, F., Cuesta-Valero, F. J., Kirchengast, G., Adusumilli, S., Straneo, F.,  
1870 Ablain, M., Allan, R. P., Barker, P. M., Beltrami, H., Blazquez, A., Boyer, T., Cheng, L., Church, J.,  
1871 Desbruyeres, D., Dolman, H., Domingues, C. M., García-García, A., Giglio, D., Gilson, J. E., Gorfer, M.,  
1872 Haimberger, L., Hakuba, M. Z., Hendricks, S., Hosoda, S., Johnson, G. C., Killick, R., King, B., Kolodziejczyk,  
1873 N., Korosov, A., Krinner, G., Kuusela, M., Landerer, F. W., Langer, M., Lavergne, T., Lawrence, I., Li, Y.,  
1874 Lyman, J., Marti, F., Marzeion, B., Mayer, M., MacDougall, A. H., McDougall, T., Monselesan, D. P., Nitzbon,  
1875 J., Otsaka, I., Peng, J., Purkey, S., Roemmich, D., Sato, K., Sato, K., Savita, A., Schweiger, A., Shepherd, A.,  
1876 Seneviratne, S. I., Simons, L., Slater, D. A., Slater, T., Steiner, A. K., Suga, T., Szekely, T., Thiery, W.,  
1877 Timmermans, M.-L., Vanderkelen, I., Wjiffels, S. E., Wu, T., and Zemp, M.: Heat stored in the Earth system  
1878 1960–2020: where does the energy go?, Earth Syst. Sci. Data, 15, 1675–1709, [https://doi.org/10.5194/essd-15-](https://doi.org/10.5194/essd-15-1675-2023)  
1879 [1675-2023](https://doi.org/10.5194/essd-15-1675-2023), 2023.  
1880  
1881 Wagener, T., Metzl, N., Caffin, M., Fin, J., Helias Nunige, S., Lefevre, D., Lo Monaco, C., Rougier, G., and  
1882 Moutin, T.: Carbonate system distribution, anthropogenic carbon and acidification in the western tropical South  
1883 Pacific (OUTPACE 2015 transect), Biogeosciences, 15, 5221-5236, <https://doi.org/10.5194/bg-15-5221-2018>,  
1884 2018.  
1885  
1886 Wimart-Rousseau, C.: Dynamiques saisonnière et pluriannuelle du système des carbonates dans les eaux de  
1887 surface en mer Méditerranée, Sciences de l'environnement. Aix-Marseille Université, [https://hal.archives-](https://hal.archives-ouvertes.fr/tel-03523187)  
1888 [ouvertes.fr/tel-03523187](https://hal.archives-ouvertes.fr/tel-03523187), 2021  
1889  
1890 Wimart-Rousseau, C., Lajaunie-Salla, K., Marrec, P., Wagener, T., Raimbault, P., Lagadec, V., Lafont, M.,  
1891 Garcia, N., Diaz, F., Pinazo, C., Yohia, C., Garcia, F., Xueref-Remy, I., Blanc, P.-E., Armengaud, A., and  
1892 Lefèvre, D.: Temporal variability of the carbonate system and air-sea CO<sub>2</sub> exchanges in a Mediterranean human-  
1893 impacted coastal site. Estuarine, Coastal and Shelf Science. <https://doi.org/10.1016/j.ecss.2020.106641>, 2020.  
1894  
1895 Wimart-Rousseau, C., Wagener, T., Álvarez, M., Moutin, T., Fourier, M., Coppola, L., Niclas-Chirurgien, L.,  
1896 Raimbault, P., D'Ortenzio, F., Durrieu de Madron, X., Taillandier, V., Dumas, F., Conan, P., Pujo-Pay, M. and  
1897 Lefèvre, D.: Seasonal and Interannual Variability of the CO<sub>2</sub> System in the Eastern Mediterranean Sea: A Case  
1898 Study in the North Western Levantine Basin. Front. Mar. Sci. 8:649246. doi: 10.3389/fmars.2021.649246, 2021  
1899

Mis en forme : Non souligné

Mis en forme : Non souligné, Couleur de police : Automatique



1900 Wimart-Rousseau, C., Wagener, T., Bosse, A., Raimbault, P., Coppola, L., Fourier, M., Ulses, C. and Lefèvre,  
1901 D.: Assessing seasonal and interannual changes in carbonate chemistry across two timeseries sites in the North  
1902 Western Mediterranean Sea. *Front. Mar. Sci.* 10:1281003. doi: 10.3389/fmars.2023.1281003, 2023.  
1903  
1904 WMO/GCOS, 2018: <https://gcos.wmo.int/en/global-climate-indicators>, 2018  
1905  
1906 Yao, M. K., Marcou, O., Goyet, C., Guglielmi, V., Touratier, F., and Savy, J.-P.: Time variability of the north-  
1907 western Mediterranean Sea pH over 1995-2011. *Marine Environmental Research*, doi:  
1908 10.1016/j.marenvres.2016.02.016, 2016  
1909  
1910 Yoder, M. F., Palevsky, H. I., and Fogaren, K. E.: Net community production and inorganic carbon cycling in  
1911 the central Irminger Sea. *Journal of Geophysical Research: Oceans*, 129, e2024JC021027.  
1912 <https://doi.org/10.1029/2024JC021027>, 2024  
1913  
1914 Zhang, S., Wu, Y., Cai, W.-J., Cai, W., Feely, R. A., Wang, Z., et al. : Transport of anthropogenic carbon from  
1915 the Antarctic shelf to deep Southern Ocean triggers acidification. *Global Biogeochemical Cycles*, 37,  
1916 e2023GB007921. <https://doi.org/10.1029/2023GB007921>, 2023  
1917